AN ABSTRACT OF THE THESIS OF

Jenna Schardt for the degree of Master of Science in Materials Science presented on June 8, 2018.

Title: The Use of Various Morphologies of Nanocellulose as Life Long Anodes of Sodium Ion Batteries.

Abstract approved: _____

John Simonsen

Sodium-ion batteries (SIBs) require the use of a highly reversible anode. To form this anode carbon nanofibers and nanocrystals are derived from cellulose nanofibers, cellulose nanocrystals, and bacterial nanocellulose. The primary structure of the cellulose nanofibers is maintained when carbonized allowing for high surface area in the structure. The carbon nanofibers exhibit promising electrochemical properties, including good rate capability (85 mA h g-1 at 2000 mA g-1), and excellent cycling stability (176 mA h g-1 at 200 mA g-1 over 600 cycles). The other morphologies show similar capacities and cycling stabilities.

The Use of Various Morphologies of Nanocellulose as Life Long Anodes of Sodium Ion Batteries

by
Jenna Schardt

A THESIS

submitted to

Oregon State University

in partial fulfillment of
the requirements for the
degree of

Master of Science

Presented June 8, 2018
Commencement June 2019

Master of Science thesis of Jenna Schardt presented on June 8, 2018

APPROVED:

Major Professor, representing Materials Science

Head of the School of Mechanical, Industrial, and Manufacturing Engineering

Dean of the Graduate School

I understand that my thesis will become part of the permanent collection of Oregon State University libraries. My signature below authorizes release of my thesis to any reader upon request.

Jenna Schardt, Author

ACKNOWLEDGEMENTS

I would like to give my sincerest thanks to Dr. John Simonsen for his patient and kind guidance over the years. He has been nothing but supportive and willing to help in the advancement of my degree and career. I would like to thank Dr. David Cann for his support and help over the past year. Dr. David Ji and his lab, particularly Dr. Clement Bommier and Dr. Wei Luo. Finally, I'd like to thank my family and friends for their support, edits, and unending love they have given me throughout this process. I owe them more thanks than words can give.

TABLE OF CONTENTS

LIST OF FIGURES

LIST OF FIGURES (Continued)

LIST OF TABLES

Chapter 1 – Introduction

1.1 Batteries and Their Background

Alessandro Volta built what is considered the original battery in March of 1800 [1]. The battery is known as a voltaic pile and is formed by stacking copper and zinc with each layer separated by brine, which acted as the electrolyte. Figure 1.1 shows this simple battery. Over the next two centuries, batteries evolved to what they are today. The battery evolved from the voltaic pile to what is known as the Daniell Cell. This battery utilized a salt bridge to move ions between the electrolyte solution while electrons move between the electrodes [1].

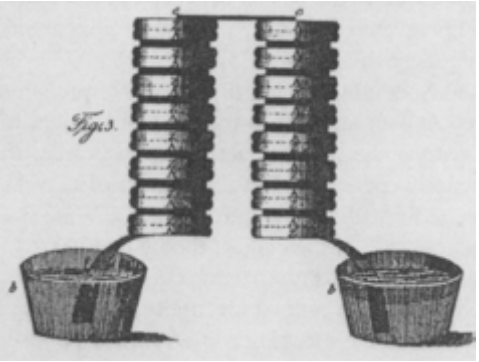

Figure 1.1.1 Drawing of Voltaic Pile [1].

The basic battery of today still consists of the two constituents of Volta's first battery: the electrolyte solution, and the electrodes. Today's batteries are divided into multiple categories with the main two being primary and secondary batteries [2]. Primary batteries are not rechargeable, whereas secondary batteries are. Primary batteries are what are used in many toys, radios, hearing aids, etc. Secondary batteries are the type of

batteries are found in many consumer electronics such as cell phones, laptops, and more recently hybrid and electric cars. Secondary batteries are also utilized in applications for storing renewable energy that can be cyclic such as such as solar and wind energy. Tesla's Solar wall is an example of a commercial product [3]. Secondary batteries, specifically sodium ion batteries (SIBs), are the focus of this thesis.

As mentioned above, batteries contain electrodes, which are divided into two groups: cathodes and anodes. Cathodes are the positive or oxidizing electrode, whereas anodes are the negative or reducing electrode. The batteries created and tested for this work utilized a simple sodium pellet as the cathode and various cellulosic materials as different tested anodes. The sodium ions move across a separator and into the anode material. All of this is suspended in an electrolyte solution. A mockup of a basic SIB battery can be found below in Figure 1.2.

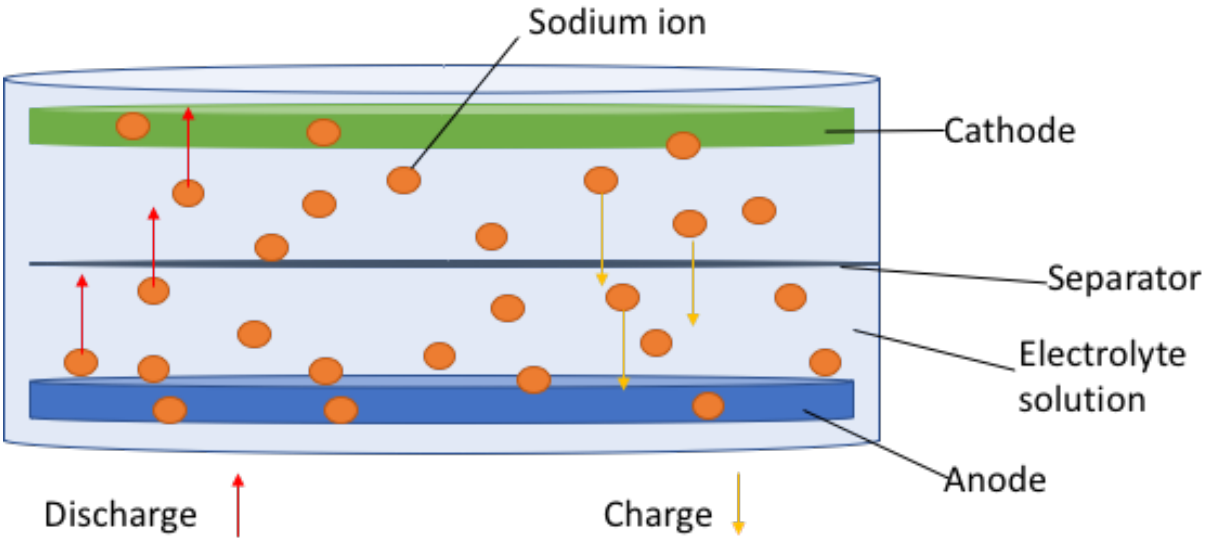

Figure 1.2 Basic Sodium Ion Battery

Batteries can be tested to measure cycling for charge/discharge cycles, performance at different amperages and various other parameters. The batteries studied here were tested for long term cycle performance, their rate cycling performance, and their cyclic

voltammetry performance. Long term cycle performance refers to the life of the battery over the course of charge/discharge cycles. Rate cycling is performed at varying rate densities to analyze the batteries' performances under high current densities. Cyclic voltammetry is to gain an understanding of the solid electrolyte interphase, the intercalation of sodium ions into the anode, as well as the potential of the electrode.

1.2 Cellulose

Cellulose is one of the most abundant organic sources on this planet being found in all plants, and many algae. It has the structure shown in Figure 1.3 [4]. Due to the abundance of cellulose, it is an excellent renewable resource for many applications.

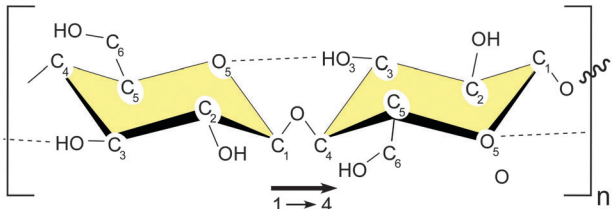

Figure 1.3 Structure of cellulose [4].

It is comprised of glucose rings that are connected via a covalent oxygen bond that bridges the C1 carbon of one ring to the C4 carbon of the neighboring ring. There are four polymorphs of crystalline cellulose, I, II, III, and IV. Cellulose I is the form of cellulose that gives rise to nanocellulose structures. Within cellulose I there are two more polymorphs, cellulose Iα which is triclinic and Iβ which is monoclinic. The configurations of these are shown in Figure 1.4[4].

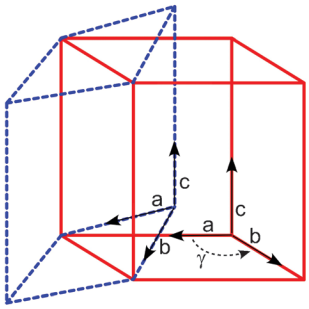

Figure 1.4 The Iα and Iβ in cellulose structures in blue and red respectively [4].

Nanocellulose is sourced from a variety of plants, animals, bacteria, and algae. In this study the cellulose was sourced from plants and bacteria. The way nanocellulose is formed renders different morphologies of the nanocellulose. Cellulose nanofibers (CNFs) are long strands of nanocellulose with very high aspect ratios that contain both amorphous and crystalline cellulose. Carboxylated cellulose nanocrystals (CCNCs) are nanorods with a lower aspect ratio compared to that of CNFs and a rice- shape containing 54-88% crystalline cellulose. They are functionalized with a carboxyl group. Sulfated cellulose nanocrystals (SCNC) are like CCNC, but the instead of being functionalized with a carboxyl group, there is a sulfate group. Bacterial nanocellulose (BNC) is most commonly sourced from the fibrils secreted by *Acetobacter*, but other bacteria can be used as well. BNC is ribbon shaped.

1.3 Carbon

Carbon has two major crystalline structures: graphite and diamond. Diamond is well known for being the hardest material. It has a distinct structure shown in Figure 1.5 [5].

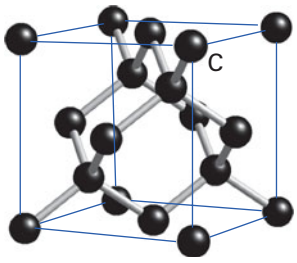

Figure 1.5 The cubic diamond structure of Carbon [5].

The anodes of many lithium ion batteries are graphitic, meaning they have the graphite structure shown in Figure 1.6b. The spacing of the graphite sheets are 0.3354 nm, is useful for lithium ion batteries because lithium ions which are 0.076 nm, and thus able to move freely between the sheets. Sodium ions, being larger at 0.102 nm have more difficulty moving between the sheets and prefer a similar, but more broken up structure called turbostratic carbon – which is shown in Figure 1.6b [6] [7]. Turbostratic carbon sheets have a spacing of about 0.4 nm at their furthest and 0.335 nm at their closest, allowing the larger sodium ions to move through with ease.

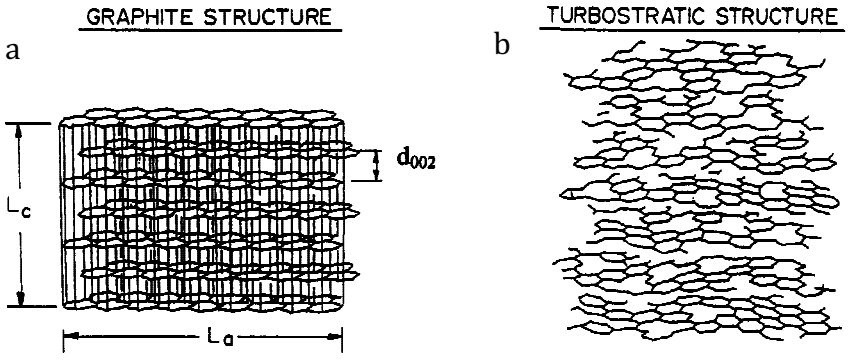

Figure 1.6 a) representation of graphene b) Representation of Turbostratic Carbon [7].

It is easy to see that the six-member ring of nanocellulose, shown in Figure 1.3 is similar to the six-member carbon ring of graphite. By using the carbon-rich structure of nanocellulose, the turbostratic structure seen in Figure 1.6b is attainable via pyrolysis.

Chapter 2 - Literature Review

2.1 Sodium Ion Batteries

In testing hard carbon anodes derived from the pyrolysis of glucose, D.A Stevens, and J.R. Dahn [8] determined that hard carbon can be used as a reversible anode for sodium ion batteries. They found that sodium ions insert reversibly at a capacity of 300 mA/g, which is close to that of lithium ions inserting into graphite. The authors observed that the sodium cells had a larger voltage across a low potential voltage than lithium did. This indicates sodium had a higher binding energy with the pyrolyzed glucose than the lithium had with it.

Sodium has a redox potential of $E°_{(Na+/Na)} = -2.71V$ when paired with the standard hydrogen electrode. This means that cell potential – the measurement in volts of the difference between the positive and negative side of the battery [2] – of sodium ions versus sodium is -2.71 V. The electrons are moving from the positive electrode to the negative electrode, causing the negative potential. Discharge is then favorable as it allows the reaction to proceed "downhill," the free energy of the occurring redox reaction [9].

Early on, research on SIBs (sodium ion batteries) was done at high temperatures to keep Na in its liquid state. These SIBs were Na/S and $Na/NiCl_2$ batteries [8]. Due to these high temperatures, the batteries were dangerous to work with and posed issues with maintaining operating temperatures. Thus, LIBs became the norm as they could be operated at ambient temperatures. Graphite was used as the basic anode for the LIBs (lithium ion batteries). When studied as an anode for SIBs, it was discovered that graphite is irreversible, and has a low capacity. Thus, making it extremely non-ideal for a reusable anode. Materials containing graphene, rather than graphite have been shown to have

promising results as reusable anodes [10]. Turbostratic carbons are a source of graphene without being graphite. They have a structure that is chaotic but contains graphitic remnants. These structures tend to have a low BET surface area, of about 3.3 m^2g^{-1}. BET is an acronym of surnames of the founders - Brunauer, Emmett, and Teller – of the method used to characterize the adsorption of gas molecules on a solid's surface[10]. This allows for a measurement of surface area. The low surface area noted above of 3.3m^2g^{-1} in the turbostratic carbon is key, and necessary for the reversibility in cycling sodium ions. When using turbostratic carbons, they should possess properties such as a small particle size, low surface area/volume ratio and a morphology that minimizes side-reaction with electrolyte at low voltages [11].

There are also non-carbonaceous anodes that have also been tested. The $Na_2Ti_3O_7$ produced 178 mAh/g at 0.3 V, 0.4 Na at 1.5 V vs Na/Na+, at 150 mAh/g, and Sn_2O_4 produced 800 mAh/h at 0.5V vs Na/Na+ for 20 cycles [11]. For testing, 20 cycles overall are generally too few to describe an entire battery life, so although it has exceptional capacity, it needs more cycles to show that it is a contender for a reusable anode.

According to N. Yabuuchi, et al., sodium and lithium ions were being studied in the 1980's as charge carriers[12]. Lithium was pursued more, most likely due to the fact that it has a higher charge density than sodium. The theoretical capacity for reversible LIBs is 372 mAh/g. Studies have shown up to 360 mAh/g in LIBs using graphite as its anodic material. In 2000, it was shown that carbonized glucose allowed Na to have a reversible capacity of 300 mAh/g. [8]. This is comparable to the reversible capacity of 350 mAh/g that L. Wei, et al. found cellulose to have thirteen years later using cellulose nanofibers [13].

Insertion and desertion was mentioned above, but N. Yabuuchi, et al., address this more in depth. They hypothesize that ions insert into ionic sites in the micropores, while Na_2 inserts to covalent sites between the graphitic layers. In reduction, the ions are intercalated into the interstitial spaces first, and then the ions fill the layers between the micropores. This has been confirmed by X-ray scattering Analysis [12].

Another important component in batteries is the electrolyte solution. Propylene carbonate electrolyte solutions have been used by S. Komaba, et al. successfully with layered hard carbon/$NaNi_{0.5}Mn_{0.5}O_2$ electrodes. But for more simplistic SIB that use solid sodium as an electrode, $NaClO_4$ and $NaPF_6$ were comparable. [14],[15]

Looking forward, the main application being considered for SIBs is large-scale energy storage batteries. Per H. Pan, et al., as of 2013, there was not sufficient evidence that hard carbon anodes were the safest route. This group suggested that considering more layered anodes such as oxides, sulfides would be better due to the cost of making hard carbons commercially. This is refuted M. Slater et al., as mentioned above, as turbostratic carbon is relatively easy to create and utilize in SIBs. [16],[11]

2.2 Cellulose

Crystalline cellulose is derived from wood, algae, bacteria, and plants. To achieve pure crystalline cellulose, the other components (hemicellulose, lignin, mantel, etc.) must be destroyed or removed from the source material. Once isolated, acid hydrolysis can be performed to rid the cellulose of amorphous areas allowing for cellulose nanocrystals to form [17]. Homogenization is another technique used to command morphology [18].This

is typically done to achieve nanofibers. Bacterial nanocellulose is secreted from *Acetobacter* – as mentioned in Chapter 1 – and often has a rectangular cross-section[19].

According to R.J. Moon, et al., crystalline cellulose has an axial modulus between Kevlar 49 and Carbon fiber – with Kevlar being 124-130 GPa, crystalline cellulose being 110-220 GPa, and carbon fiber being 150-500 GPa. The strength of crystalline cellulose is noteworthy as it retains its structure and partially its strength when freeze dried and turned into aerogels [4].

These aforementioned morphologies can all be dried via freeze-drying to create aerogels [19], [20]. Freeze drying the various types of nanocellulose allows for the aerogels to be flexible and porous. The porosity of freeze-dried cellulose nanofibers has been shown to be microporous- meaning the pore size is less than 2 nm in diameter [20], [21]. The microporosity allows for high surface area on the fibers compared to a material like carbon nanotubes which mesoporous meaning the or size is between 5-70 nm [22]. Applied to batteries, this allows for a great interface with the electrolyte solution, which allows for increased electron and ion flow across the battery [23].

Though use of pyrolysis, nanocellulose can shed its –OH groups and become a hard carbon aerogel. Pyrolysis is thought to occur in four stages: 1) release of previously absorbed water, 2) splitting off of water 3) breaking of C-O and C-C bonds, and 4) formation of layers (Turbostratic and graphitic). These steps were outlined at low temperatures (250-600°C) by M.M. Tang and R. Bacon in the 1960's [24].

Chapter 3 – Materials and Methods

Four types of cellulose were used to create anodes for the cells for comparison to industry standard carbon and wood for controls. Every "nano" sample was freeze dried.

3.1 Freeze Drying

Two freezers were used to prepare samples: a Labconco FreezeZone 4.5 and a VirTis Lyophillizer. Prior to freeze drying, all samples had 1% tert-Butyl alcohol (VWR) stirred into their liquid state and were then frozen overnight. The samples were then placed in the freeze dryer for 3 days.

3.2 Active Mass Materials

The loading masses for all the batteries are found in Table 1.

CNF

Cellulose nanofibers (CNF) were provided from Chuetsu Pulp and Paper, and were sourced from soft wood bleached kraft pulp. There were three levels of fibrillation, which allowed for three different widths of the fibers. In their pre-carbonized state "low fib" CNFs had diameters of 48.18 nm with a starting percent solids of 15.86%, "med fib" CNFs had diameters of 33.36 nm with a starting percent solids of 15.69%, and finally "high fib" CNFs had an average diameter of 21.53 nm and a starting percent solids of 12.29%. Chuetsu Pulp and Paper made these fibers by homogenizing the fibers more (low fib) or less (high fib).

The CNFs were all diluted from their original starting percent solids to 1% by adding reverse osmosis deionized(RODI) water (Omnipure K series) and sonicating for 2 hours. Samples were then placed into the freezer for freeze drying steps. Post-freeze drying, size characterization was via SEM at the OSU electron microscope facility using a FEI Helios Nanolab 650.

CCNC

Carboxylated cellulose nanocrystals (CCNC) were made in the lab. Ground Whatman cotton filter paper was used as the starting material. 50.0 g of starting material was added to a 2-liter three neck round bottom flask (RBF) with 200 mL of 12.1 N HCl (VWR). Under nitrogen, the suspension was heated to 100˚C and stirred for 2 hours. The suspension was then removed from heat and nitrogen. 1500 mL of RODI water was added and left to settle in the hood for three hours. The liquid was then decanted, and the precipitate was moved to a 6L Erlenmeyer flask and filled with RODI water to the 6L mark. After settling overnight, the liquid was siphoned off and the pellet then filtered through vacuum filtration using 25 μm Whatman cotton filters. The pellet was filtered until a pH of 6.5 was reached.

Following this, the pellet was transferred into a 3L RBF. 500 mL RODI water, 10.0 g NaBr (VWR), and 3.0 g TEMPO (VWR) were added. The RBF was then stirred while approximately of 150mL 4.0 M NaOH (VWR) and 400 mL bleach (hy-top) were added dropwise over the course of 4-6 hours. 100 mL of methanol was added to quench the reaction. The 3L RBF was left in the hood over night to allow contents to settle. The liquid was decanted, and the pellet diluted with 500 mL RODI water. The new suspension was spun down and rinsed twice via centrifuge for 1 hour to remove as much excess TEMPO,

NaOH, NaBr, and bleach as possible. The pellet was re-suspended in 500 mL RODI water and placed in dialysis for 3 days with the DI water being changed daily.

The suspension of C.CNC was then characterized by percent solids and conductivity titrations. Percent solids were found by taking the initial weight of the suspended solution of DI water and C.CNC, evaporating the water, and then weighing the remains. The weight of the remaining solids was divided by the initial weight then multiplied by 100 giving the percentage of solids in the solution. This was done in triplicate for each batch.

For the conductivity titrations, 4 mL 0.1 M HCl was added to approximately 10 g of the CCNCs (note this is the weight of the solid not the volume of the solution). 0.1 N NaOH was added dropwise at a rate of 30 mL/hr with a New Era Syringe Pump and 50 mL Chance syringe. Using a Thermo Scientific 011050MD conductivity probe connected to a VWR Symphony reader, the output of the conductivity measurements was read by a LABVIEW program written by Milo Clauson. A sample of the plot and calculations can be found in appendix A. Conductivity measurements were done to determine the carboxyl groups attached to the cellulose nanofibers – what makes them CCNC versus SCNCS.

Size characterization was done with dynamic light scattering (DLS) using the Brookhaven Instruments Corporation (BIC) BI-200SM Multiangle Research Goniometer alongside a BI-9000 AT Autocorrelator. Temperature was maintained at 25°C via a polyScience temperature controller. BIC BI_DLSW Dynamic light scattering software was used for numerical analysis.

Confirmation of the sizes were done via a FEI Titan 80-200 transmission electron microscope (TEM). The grids used were Ted Pella PELCO Formvar 400 mesh copper grids. The grids were plasma charged in a Ted Pella PELCO easiGlow glow discharge instrument to achieve hydrophilicity. 2 µL drops of 0.01%-0.05% solids solution of the various samples

were dropped onto grids. The drops of solution were allowed to dry for 5 minutes. After 5 minutes the remaining solution was wicked off with a small strip of Whatman filter paper. The samples were then stained with 2 μL of 1% phosphotungstate (PTA) for 1 minute until being wicked off again with Whatman filter paper. The samples were imaged at 200 kV.

SCNC

Sulfated cellulose nanocrystals (SCNC) were purchased from the University of Maine. SCNCs were sourced from prehydrolysis kraft dissolving pulp. 10.5% solids were diluted down to 1% solids using RODI water and sonicated for 1 hour. DLS was used to confirm the SCNCs were in fact nano, and the size distribution was correct. After this, the samples were freeze dried and characterized via SEM imaging.

BNC

Bacterial Nanocellulose was made by Camille Freitag for Dr. Simonsen's lab. In a stainless-steel bucket, the following was added: 120 g glucose, 30 g yeast extract, 30 g peptone, 16.2g anhydrous dibasic sodium phosphate, 6.9 g citric acid monohydrate, 6 L distilled water to create a medium for cultivating BNC. The pH of this mixture was adjusted to 4.5 by adding dilute HCL dropwise. 475 mL of the medium was added to cake pans, and each pan was placed in an autoclave bag, closed with wooden clothespins. The pans were autoclaved for 20 minutes. After the pan cooled it was opened in the hood. The inoculum was transferred from the tube culture via sterile transfer pipette. The bag was then sealed

and inflated via a needle attached to the compressed lab air. The bag and pan were then placed in an incubator at 28° C until pan was covered with secreted BNC.

A 3 L flask containing 2 L NaOH was heated to 90° C. After incubation, the sheets of BNC were placed into the flask for 15 minutes. The sheets were then transferred to 2 L of 1% acetic acid. After neutralizing in the acetic acid, the sheets were again transferred, this time to distilled water. The sheets were then rinsed with running distilled water and stored in a large beaker of RODI water in the refrigerator.

Size characterization of BNC was done with the SEM post freeze drying.

Wood

Douglas Fir (*Pseudotsuga menziesii*) wood chips were provided by the Wood Science Engineering department. The wood was imaged via SEM prior to carbonization. The wood was used as a macro control to the nanocellulose samples as wood is easily obtainable and is a source material for nanocellulose.

Sawdust

A mixture of wood saw dust was also used a macro control. Multiple, hard and softwoods made up the sawdust, so it is considered a randomized macro sample.

Industry standard

An industry standard for carbon anodes was provided by Sharp. CarbotronP is product from Kureha Corporation and is used in LIBs. It is a hard carbon source. This was used as another control to compare the nanocellulose to something already on the market.

3.3 Creation of electrodes and electrolyte

Pyrolysis

All materials were carbonized in their dry state – whether that was freeze dried or as is. The exception to this being CarbotronP, which was used as is. The materials were placed in ceramic crucibles and pyrolyzed under Argon for 6 hours at 1100°C in an MTI OTF-1200X tube furnace.

Cathode Materials

Pure sodium pellets were pressed and punched out inside the glove box under gaseous N_2 for use as the cathode in the batteries.

Anode materials

To create the anode, the active mass – post carbonized nanocellulose - was mixed with carbon black, polyvinylidene fluoride (PVDF), and N-Methyl-2-pyrrolidone (NMP) in

an 8:1:1 ratio. The mixture was stirred for 20 minutes with a mortar and pestle. After combined, the solution was rolled into a thin layer on a copper sheet. This sheet and solution was then dried in a drying oven for 30 minutes.

Electrolyte Solution

1M sodium perchlorate salt was placed in a 1:1 weight ratio of ethylene carbonate and propylene carbonate to create the electrolyte solution.

3.3 Battery composition

The batteries were composed inside the aforementioned glove box, again under N_2. The anode cut out was placed into the bottom cap carbon face up. A glass fiber separator was placed on top of the anode. Using a sterile glass pipette, the electrode was flooded with electrolyte solution. The cut-out sodium pellet was then placed on top of the separator. A simple spring and the top cap were placed on top of the sodium to close the battery. The battery was then crimped closed. Prior to removing the battery, it was wiped down to ensure no atmospheric interactions would occur outside of the glove box. The battery size is equivalent to a standard 2032 cell battery found in many watches and timers.

3.4 Testing

An Arbin BT2000 system was used for galvanostatic charge/discharge scanning rate

of 0.2 mV/s at room temperature. A Maccor was used for testing using a rate cycling and long term testing.

Batteries were rate tested at the following rates for 10 cycles at each rate: tested 20 mA/g, 40 mA/g, 100 mA/g, 200 mA/g, 500 mA/g, 1000 mA/g, 2000 mA/g, and 5000 mA/g.

For long cycling, the batteries were all tested at 250 mA/g over the course of 1000+ charge/discharge cycles.

Chapter 4 – Results and Discussion

4.1 – SEM and TEM images

Figures 4.1 – 4.8 show the anodic materials pre- and/or post-pyrolysis. It should be noted that the primary structure is intact within all the materials as indicated by the following SEM images. This is important, as high surface areas of the nano-materials are needed for life long anodes.

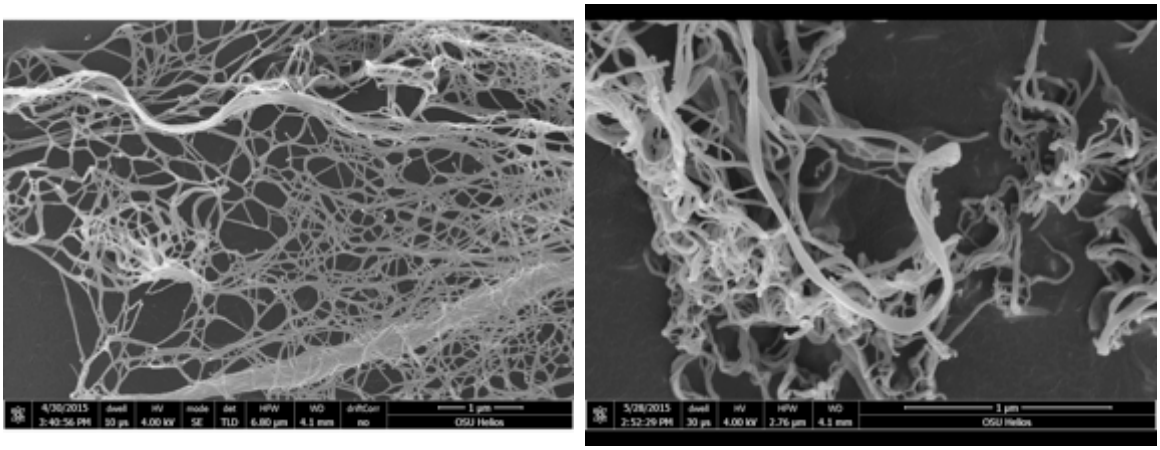

Figure 4.1 The left image shows CNF Low Fib pre-pyrolysis and the right post pyrolysis.

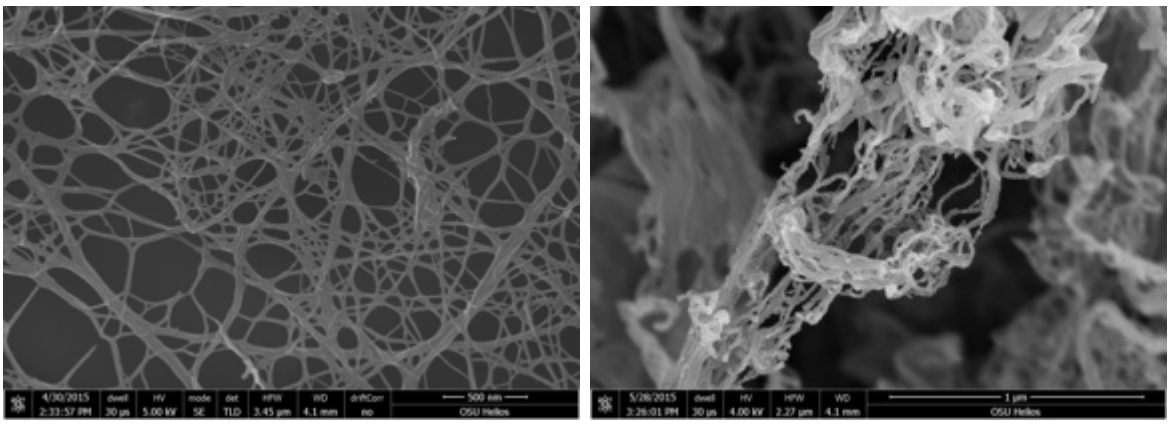

Figure 4.2 The left image shows CNF Med Fib pre-pyrolysis and the right post pyrolysis.

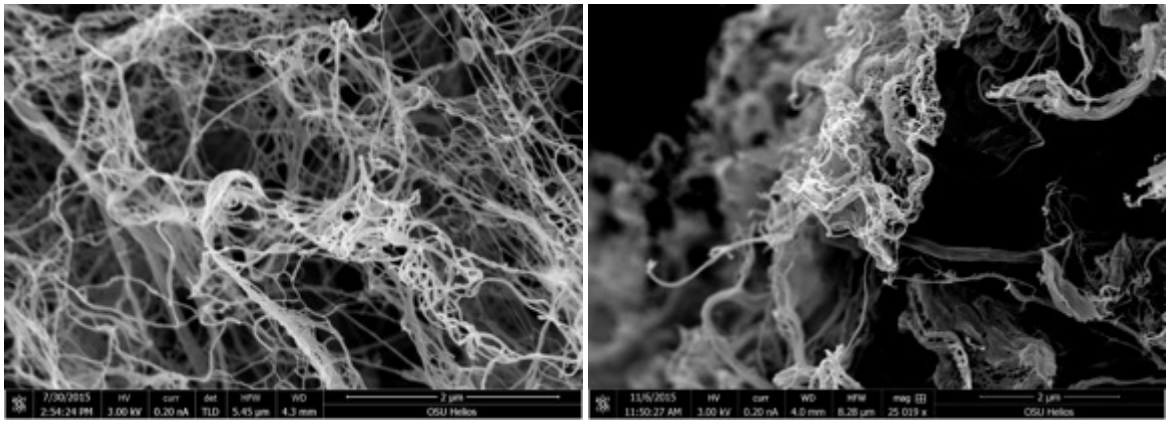

Figure 4.3 The left image shows CNF High Fib pre-pyrolysis and the right post pyrolysis.

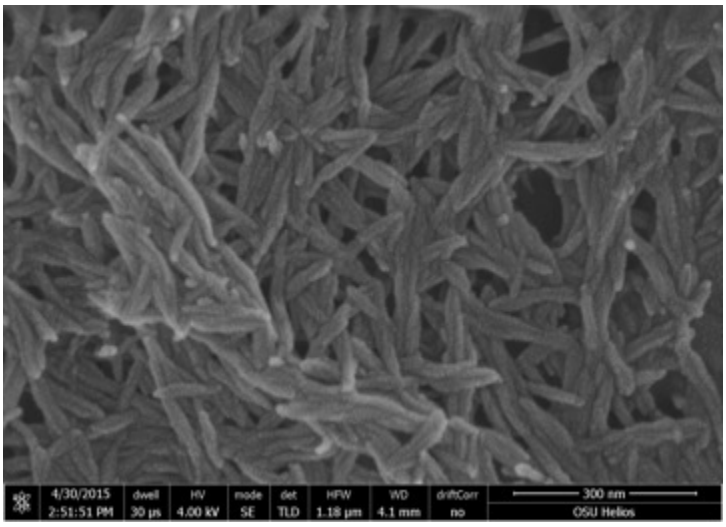

Figure 4.4 CCNC pre-pyrolysis SEM image.

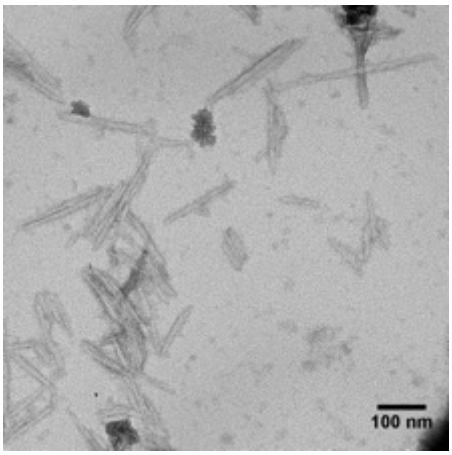

Figure 4.5 SCNC pre-pyrolysis TEM image

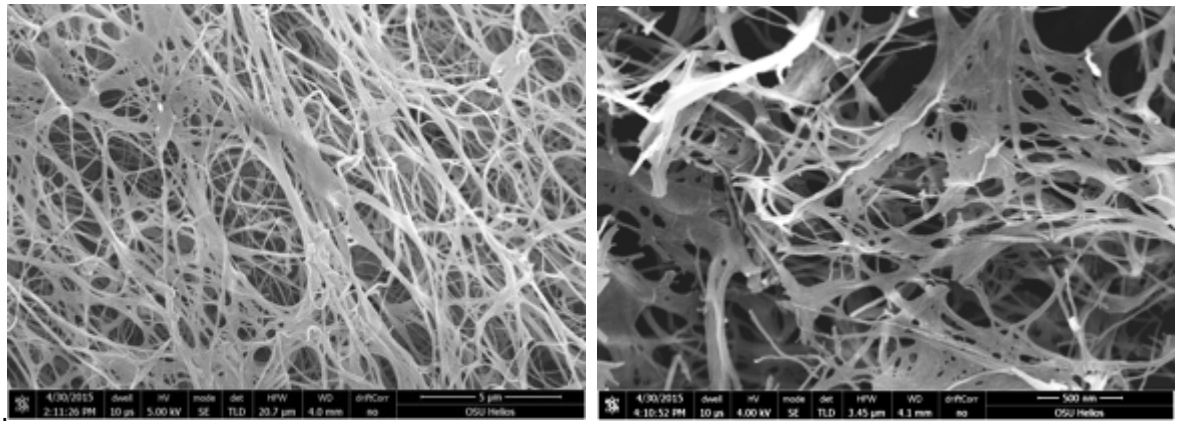

Figure 4.6 The left image shows BNC pre-pyrolysis and the right post pyrolysis.

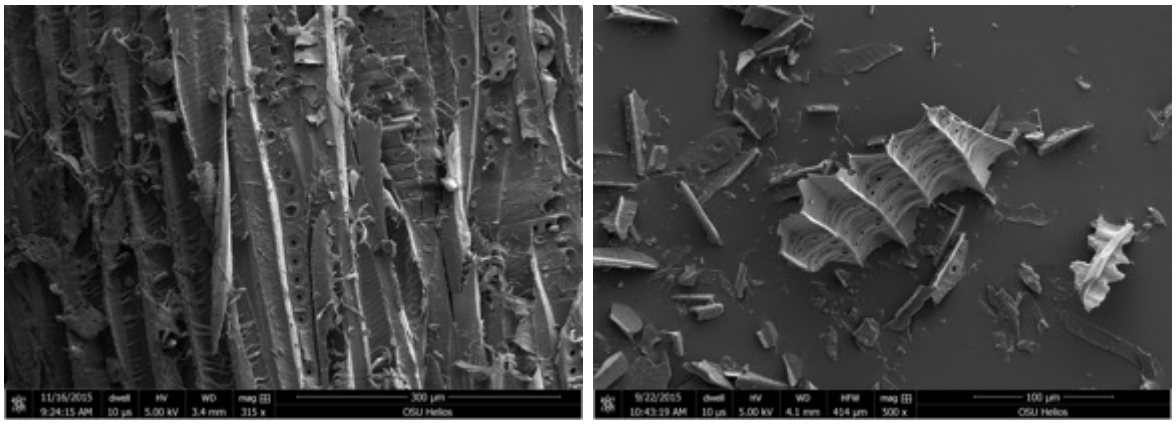

Figure 4.7 The left image shows Wood pre-pyrolysis and the right post pyrolysis, note: the wood was ground after pyrolysis with a mortar and pestle.

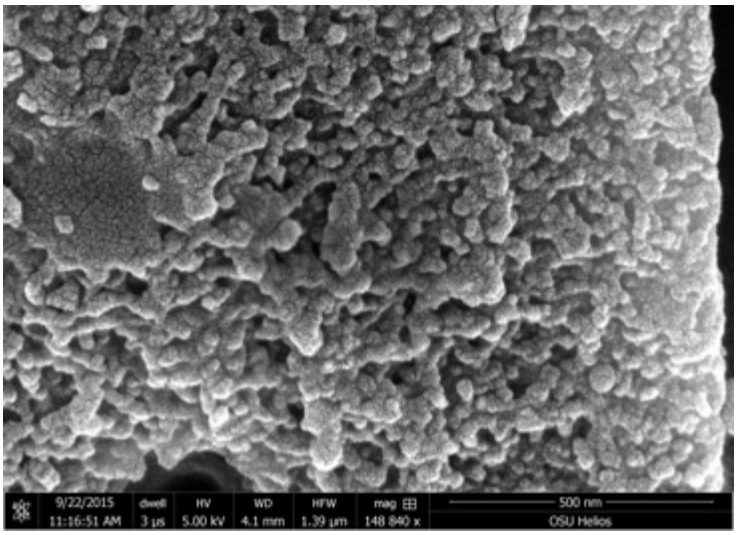

Figure 4.8 CarbotronP.

Images of CCNC and SCNC post pyrolysis could not be obtained due to a material shortage.

Table 4.1 shows the average diameter of the three different sized fibers as well as BNC pre- and post- pyrolysis. This should be kept in mind for the following testing results.

Table 4.1: Comparison of diameter size of fibers and BNC

Material	Pyrolysis	Average Diameter	St. Dev.
CNF Low Fib	Pre	25.4633	8.1248
	Post	23.9169	5.839
CNF Med Fib	Pre	17.2419	3.2414
	Post	16.1139	1.9339
CNF High Fib	Pre	15.5134	2.532
	Post	12.6121	2.1128
BNC	Pre	71.8849	26.0808
	Post	17.5145	4.8747

4.2 – Rate Cycling

Rate cycling was performed to determine how well the batteries performed under high current density. Figures 4.9-4.17 show the rate cycling of the anode materials. The current rate changed every five charge/discharge cycles and can be seen below in Table 4.2.

Table 4.2: Current rate for rate cycle testing of the batteries

Cycle number	Current rate (mA/g)
1-5	20
6-10	40
10-15	100
16-20	200
21-25	500
26-30	1000
31-35	2000
36-40	3000

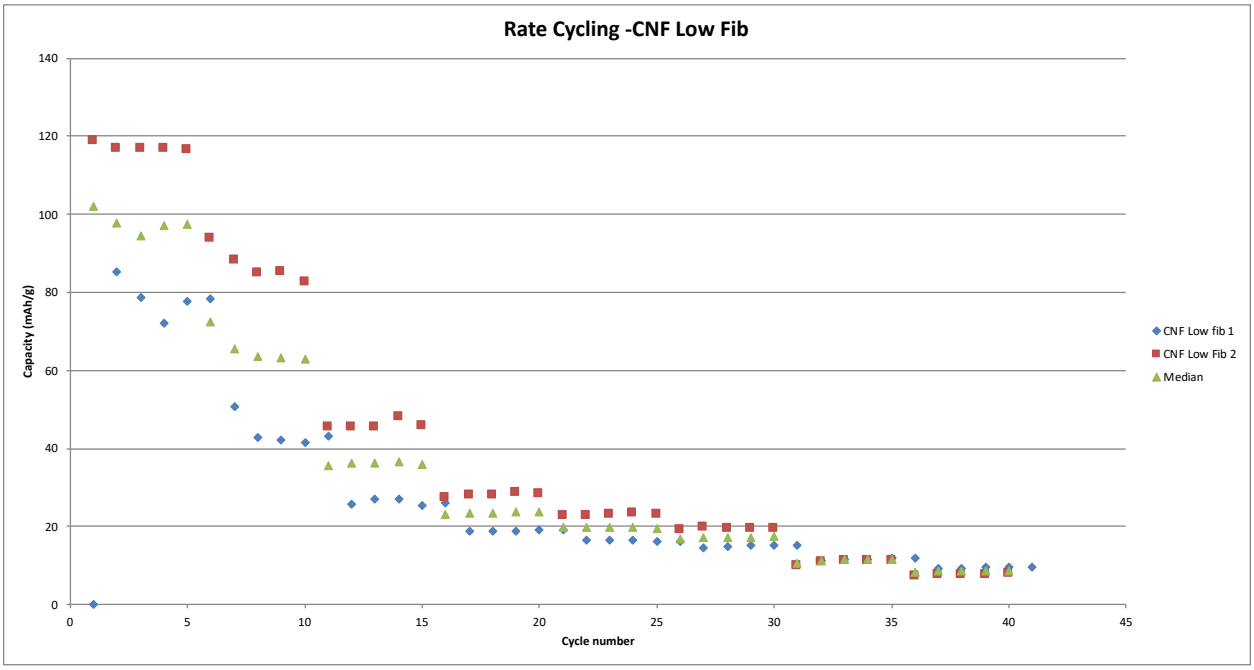

Figure 4.9 Rate Cycling for CNF Low Fib over 50 cycles.

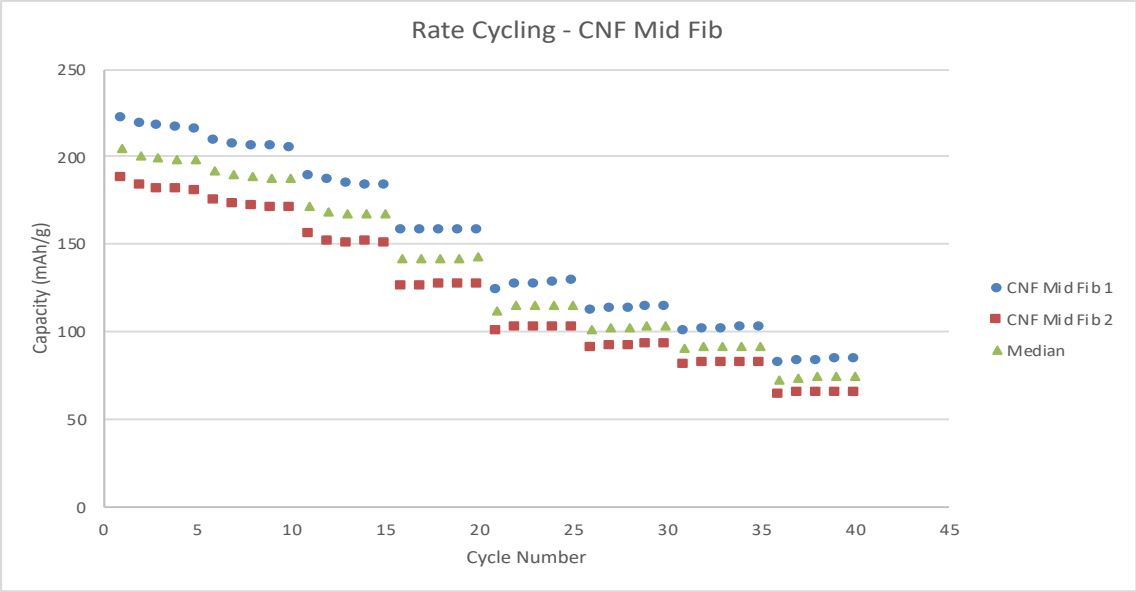

Figure 4.10 Rate Cycling for CNF Med Fib over 40 cycles.

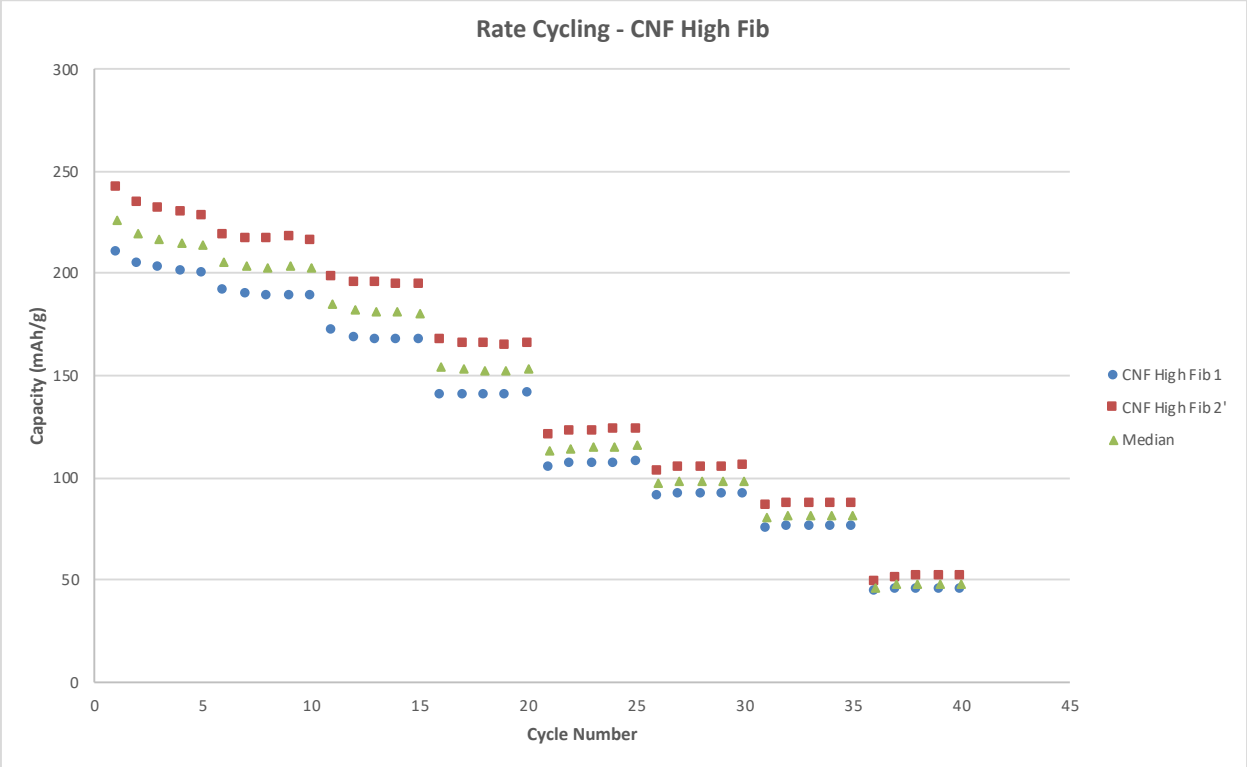

Figure 4.11 Rate cycling for CNF High Fib over 40 cycles.

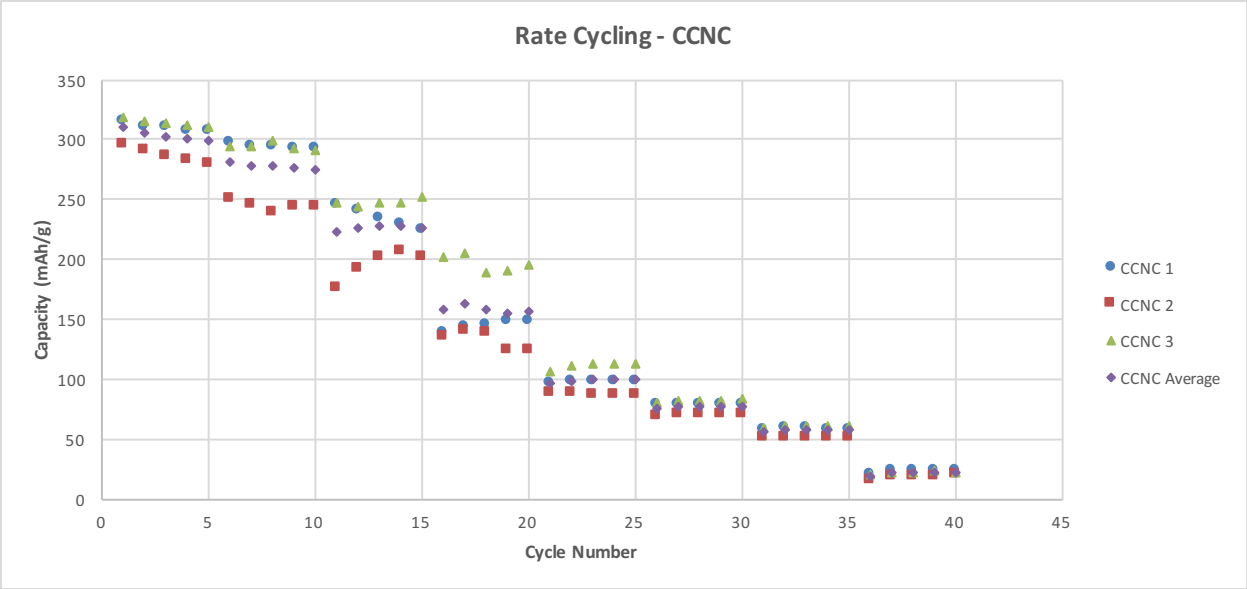

Figure 4.12 Rate Cycling for CCNC over 40 cycles.

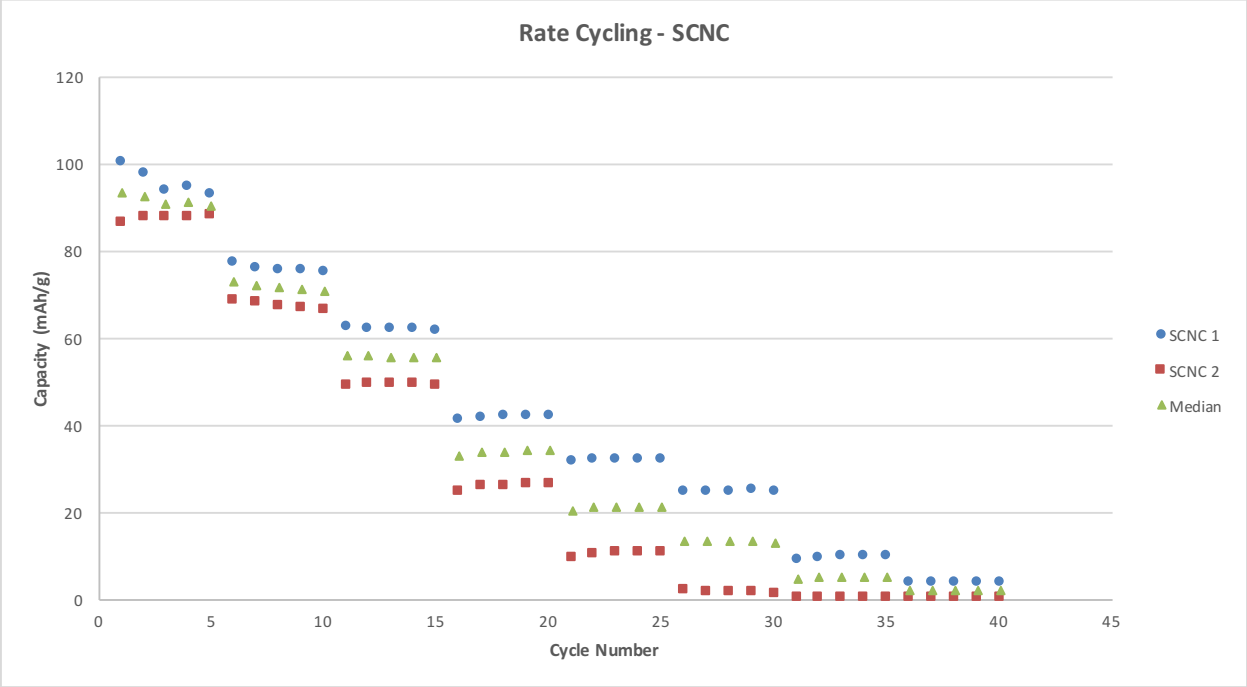

Figure 4.13 Rate Cycling of SCNC over 40 cycles.

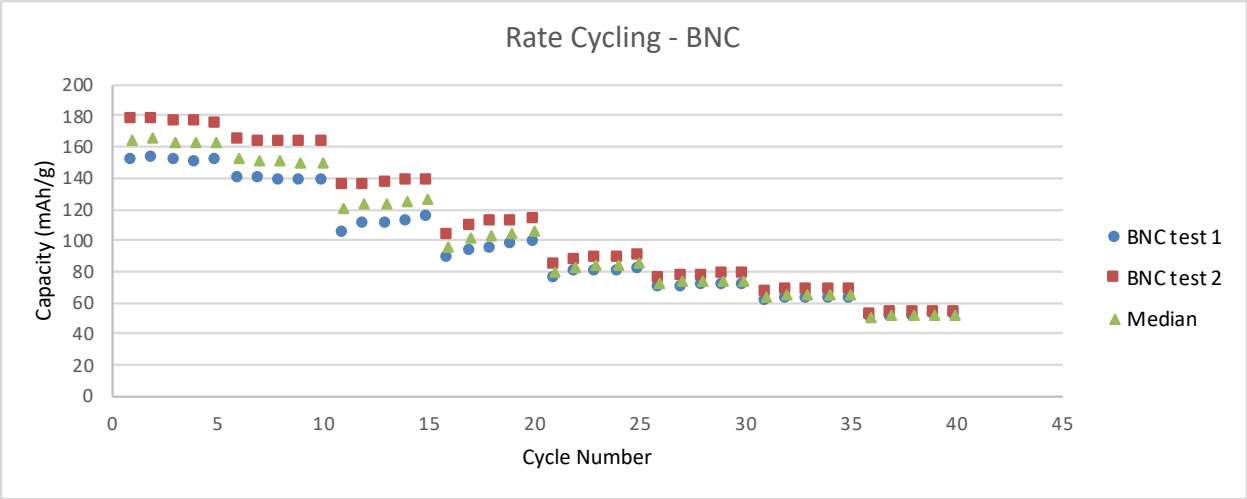

Figure 4.14 Rate Cycling of BNC over 40 cycles.

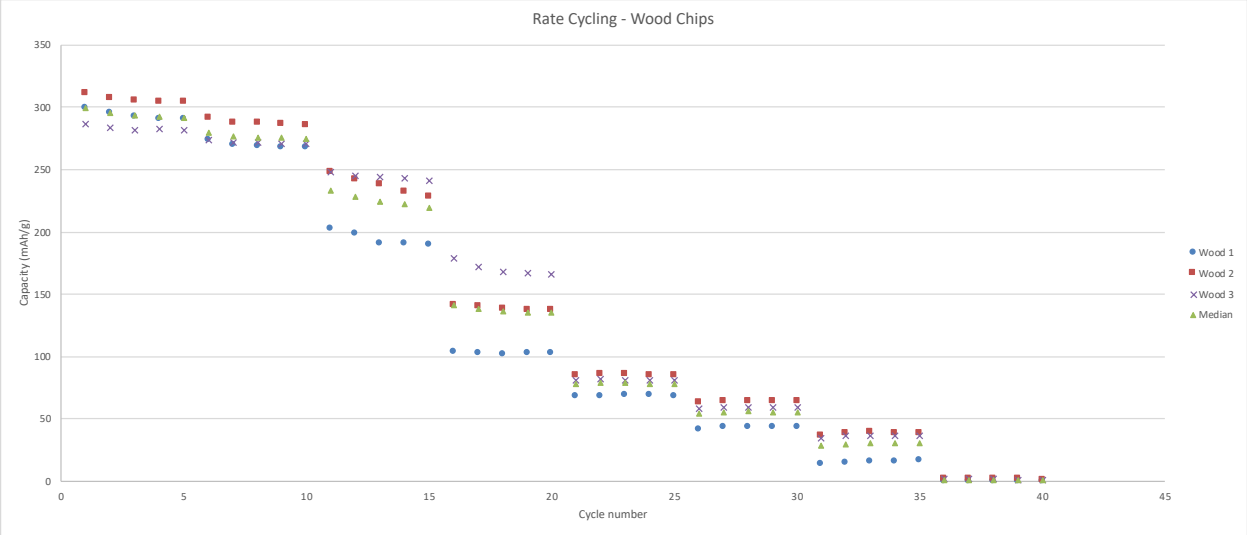

Figure 4.15F Rate Cycling of wood chips over 40 cycles.

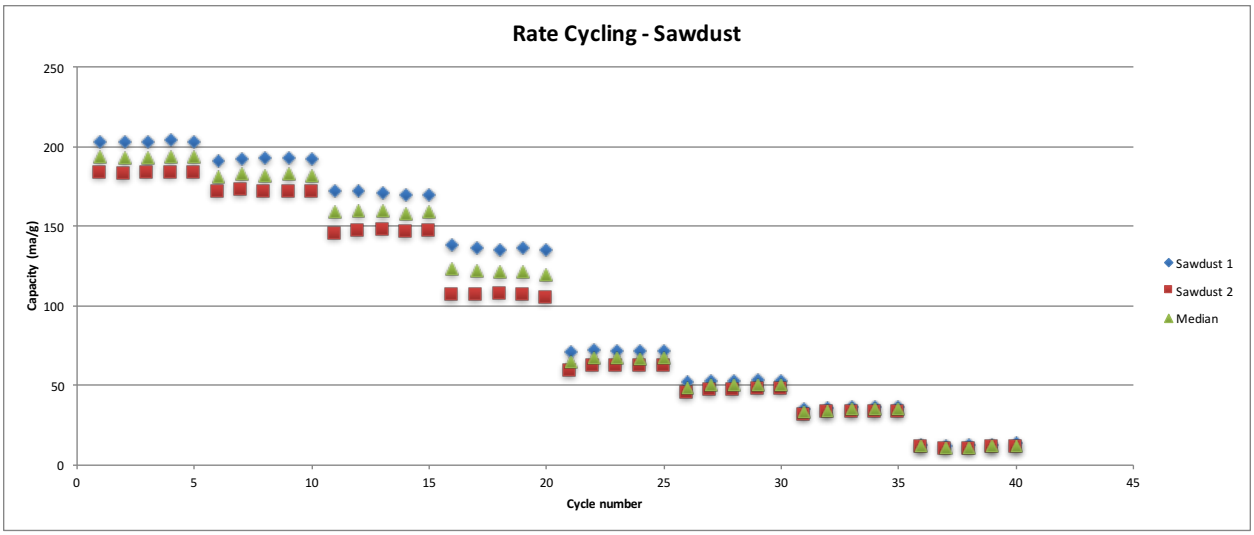

Figure 4.16 Rate Cycling of Sawdust over 40 cycles.

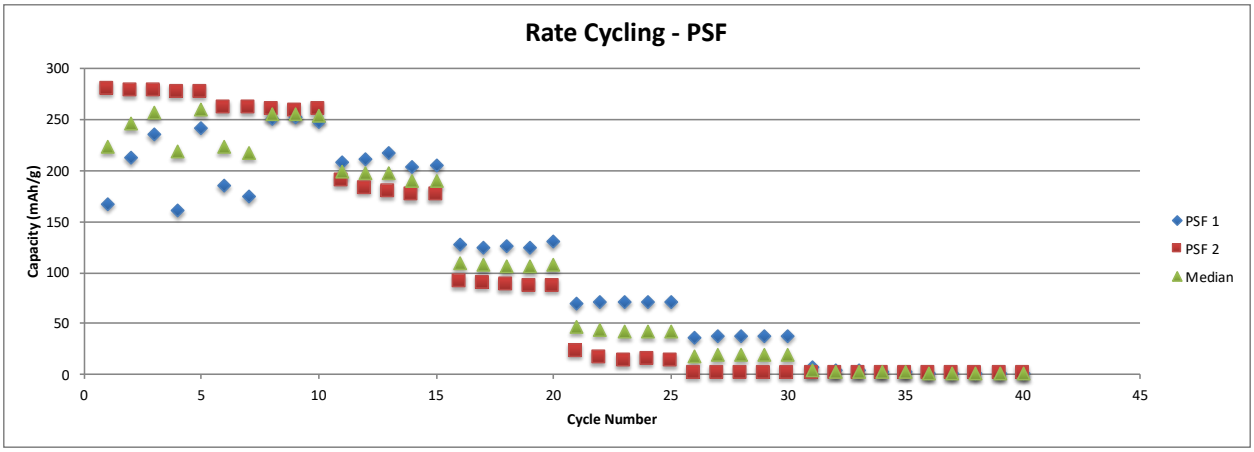

Figure 4.17 Rate Cycling of Carbotron over 40 cycles.

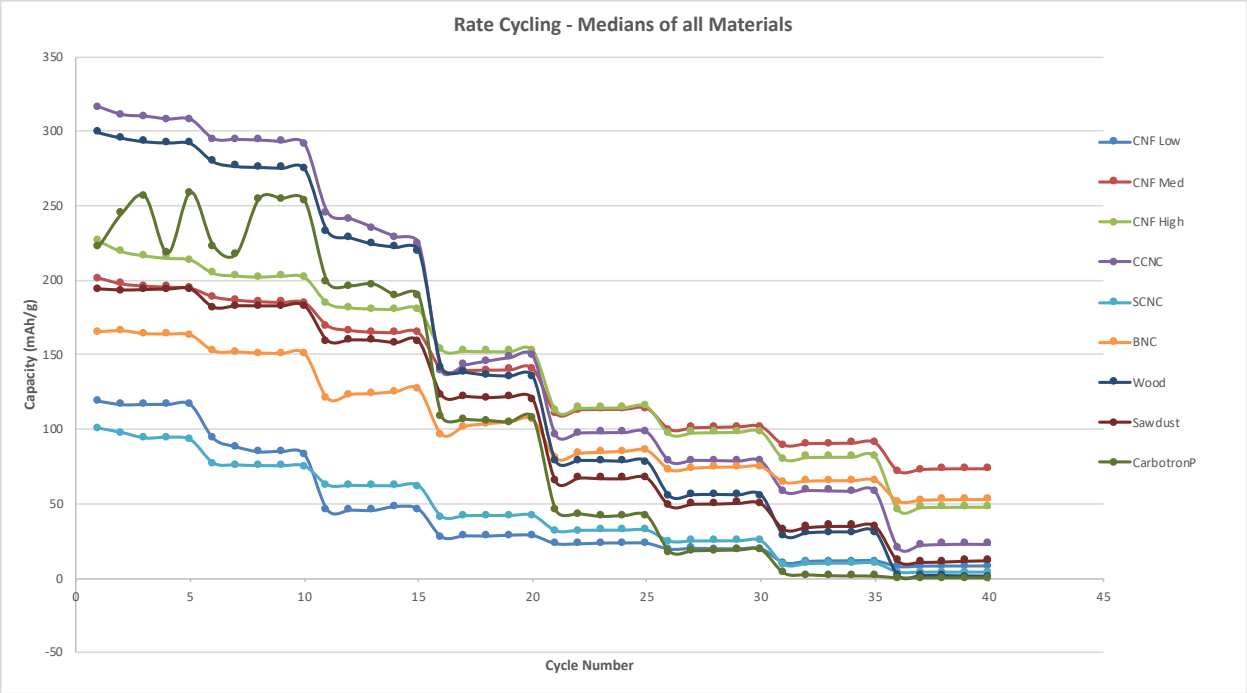

Figure 4.18 Medians of all materials rate cycling over 40-50 cycles.

CCNC performs the best at lower current density than the other anode materials, but CNF Mid performed the best at the highest current densities. CCNCs have sodium cation as the counter ion for the carboxyl group from the carboxylation procedure outlined in chapter 3. Because of this, the Na+ from the cathode has an easier time inserting in to the anode over the first cycles.

CNF Mid Fib performs the best at high current densities. The low diameter is similar to that of the other CNFs and BNC. The Med Fib fibers are almost identical to the Large Fib fibers in terms of diameter but have been homogenized longer. It is interesting to note that the CNF High and BNC performed very closely at high current densities, even though BNC did not perform as well at the lower density currents as CNF High. This may be due to post- pyrolysis spacing of the carbon chains.

4.3 – Galvanostatic Charge/Discharge Plots

Galvanostatic tests were performed on all the batteries at a current of 40 mA/g and with a potential of 0.1 V-2 V. On each plot the first cycle is noticeably different than the rest. This is the due to a solid electrolyte interphase (SEI) forming. The SEI shows the ions tunneling into the anode material and finding the best paths for all future cycling. In the following 4 cycles, it is seen that there is a lessening in activity. This is due to the sodium ions intercalating between the graphene layers of the anode. Figures 4.19 – 4.27 show the Galvanostatic tests of cycles 1-5, 10, 50, 100, 250, 500, 750, and 1000 for the anodic materials. Where figures 4.28 and 4.29 show the first cycle and 500th cycles for all the materials.

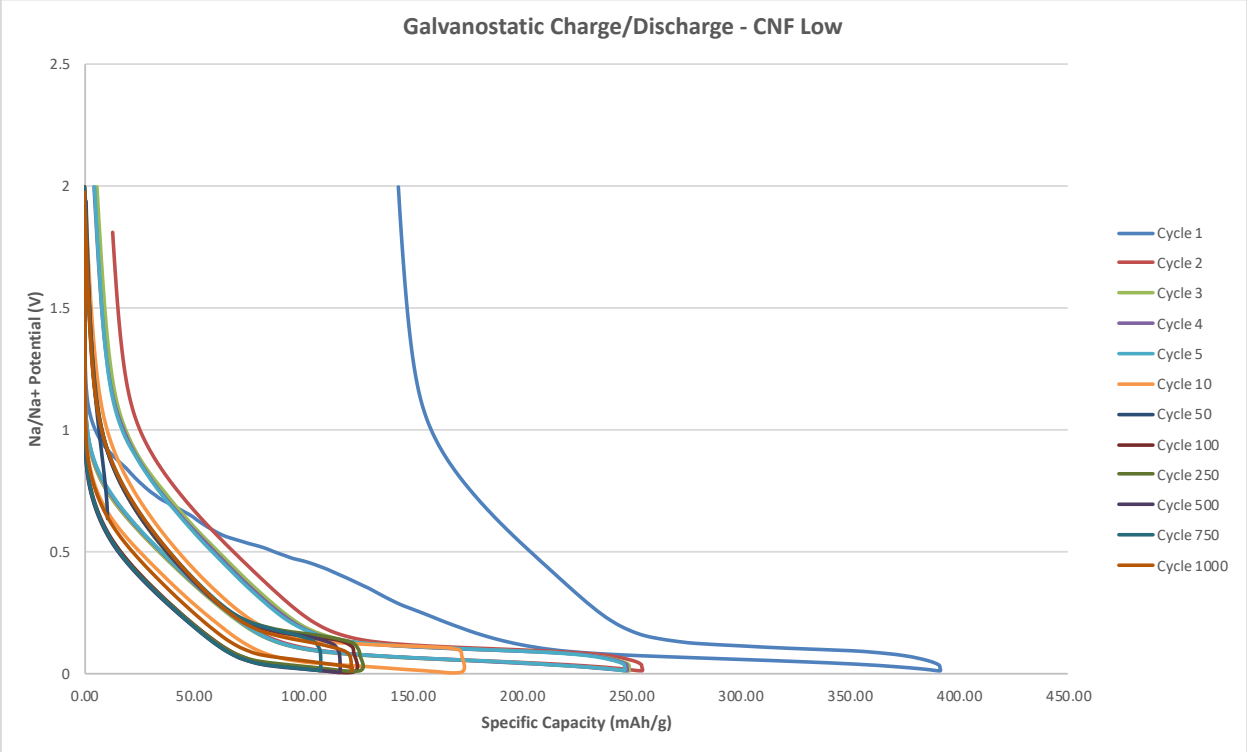

Figure 4.19 Galvanostatic charge/discharge cycles of selected cycles of CNF Low Fib.

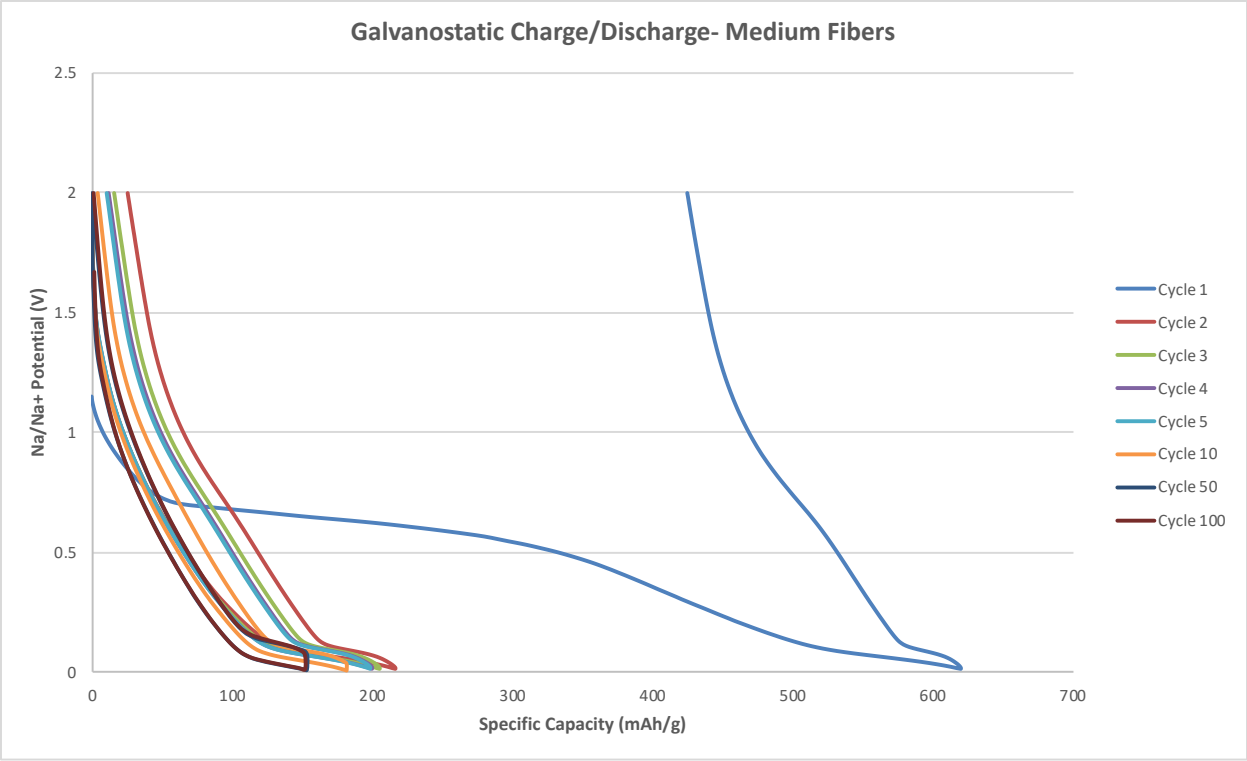

Figure 4.20 Galvanostatic charge/discharge cycles of selected cycles of CNF Med Fib.

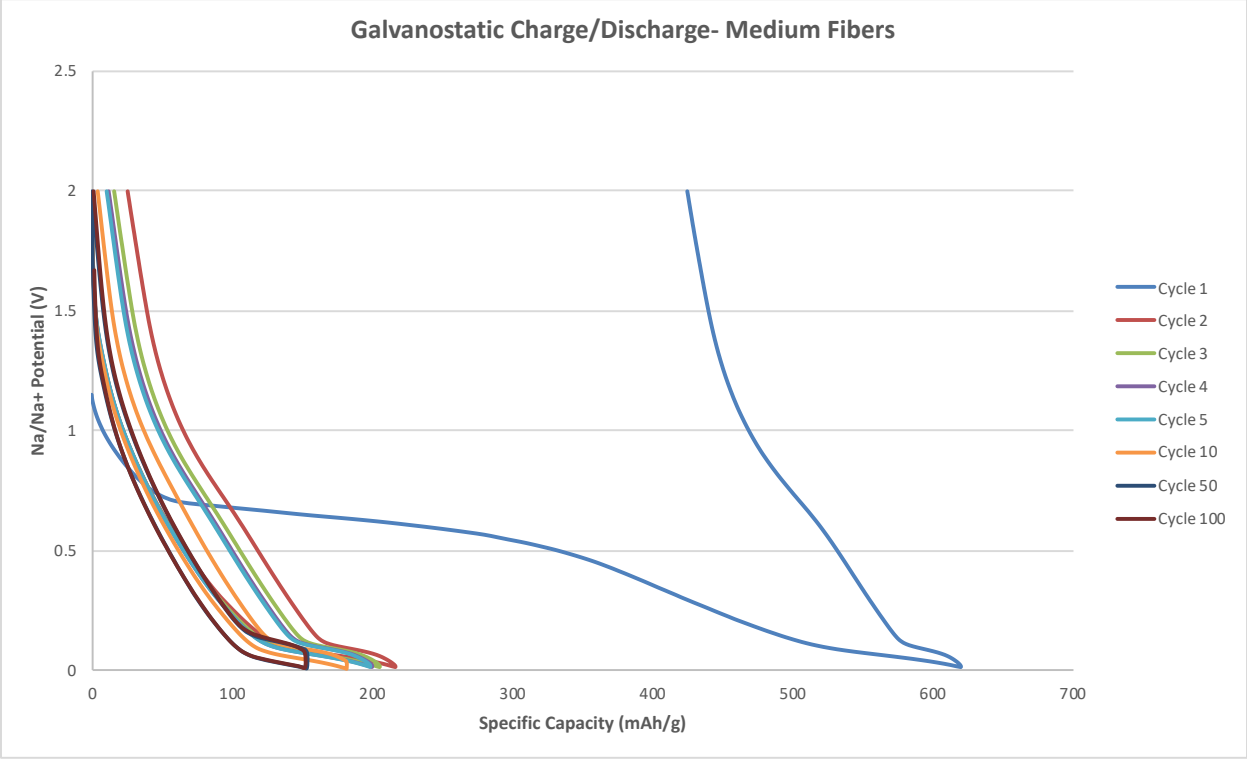

Figure 4.21 Galvanostatic charge/discharge cycles of selected cycles of CNF High Fib.

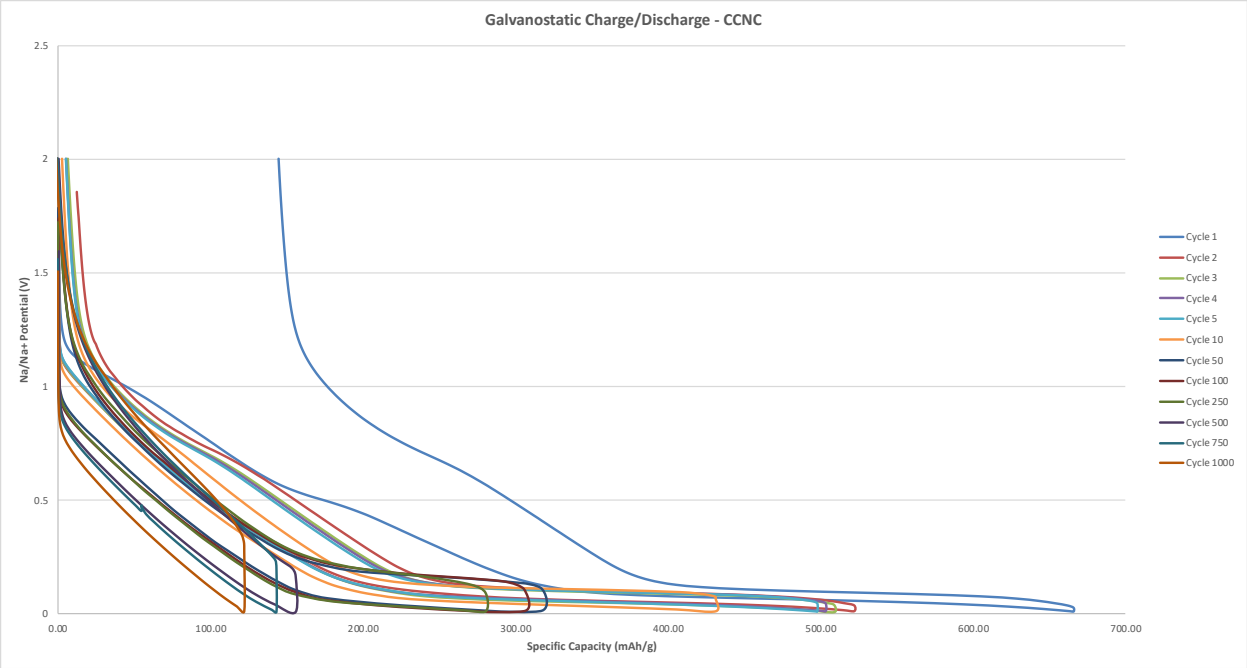

Figure 4.22 Galvanostatic charge/discharge cycles of selected cycles of CCNC.

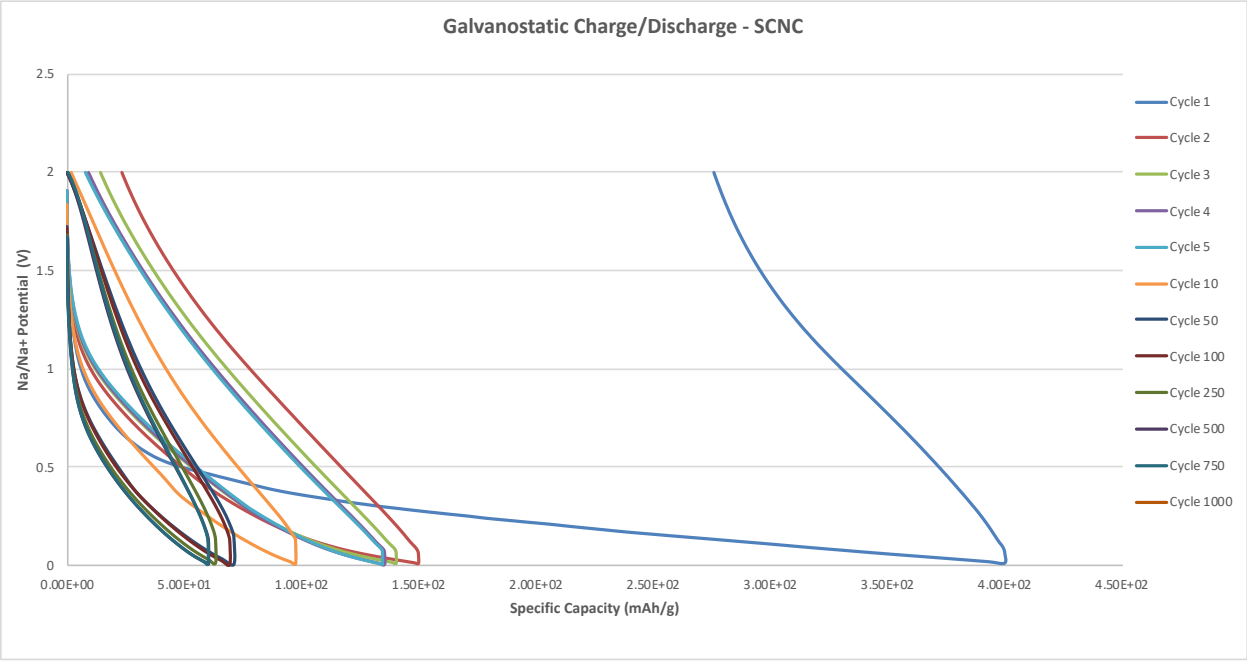

Figure 4.23 Galvanostatic charge/discharge cycles of selected cycles of SCNC.

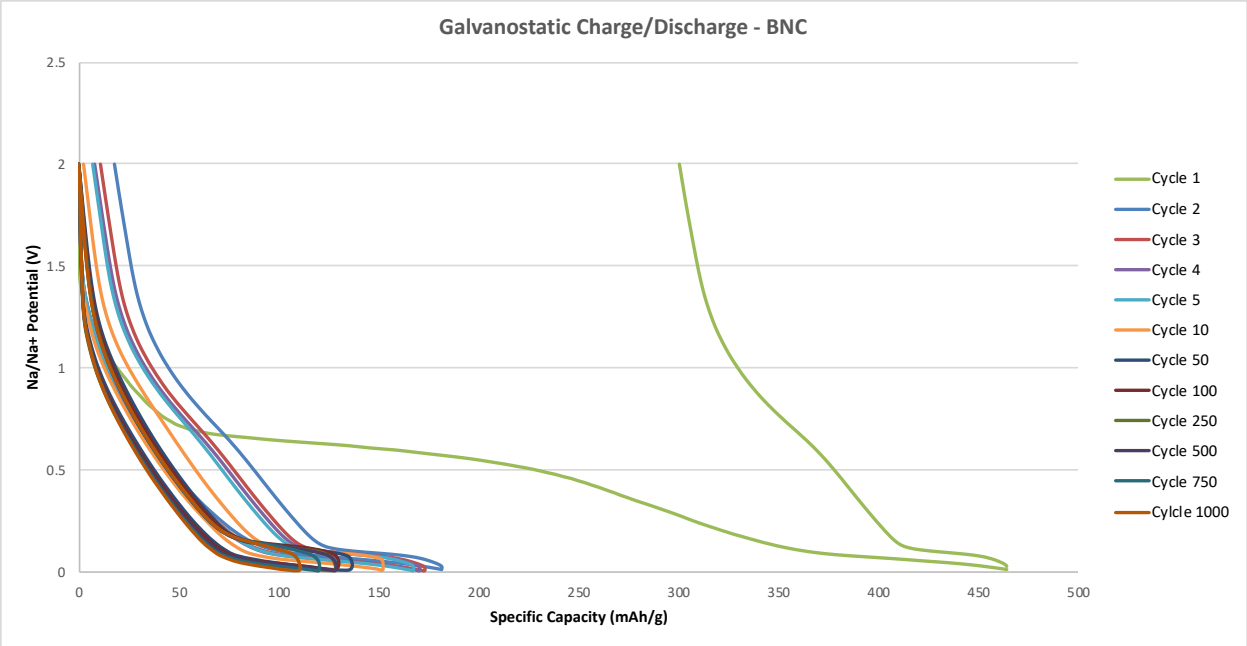

Figure 4.24 Galvanostatic charge/discharge cycles of selected cycles of BNC.

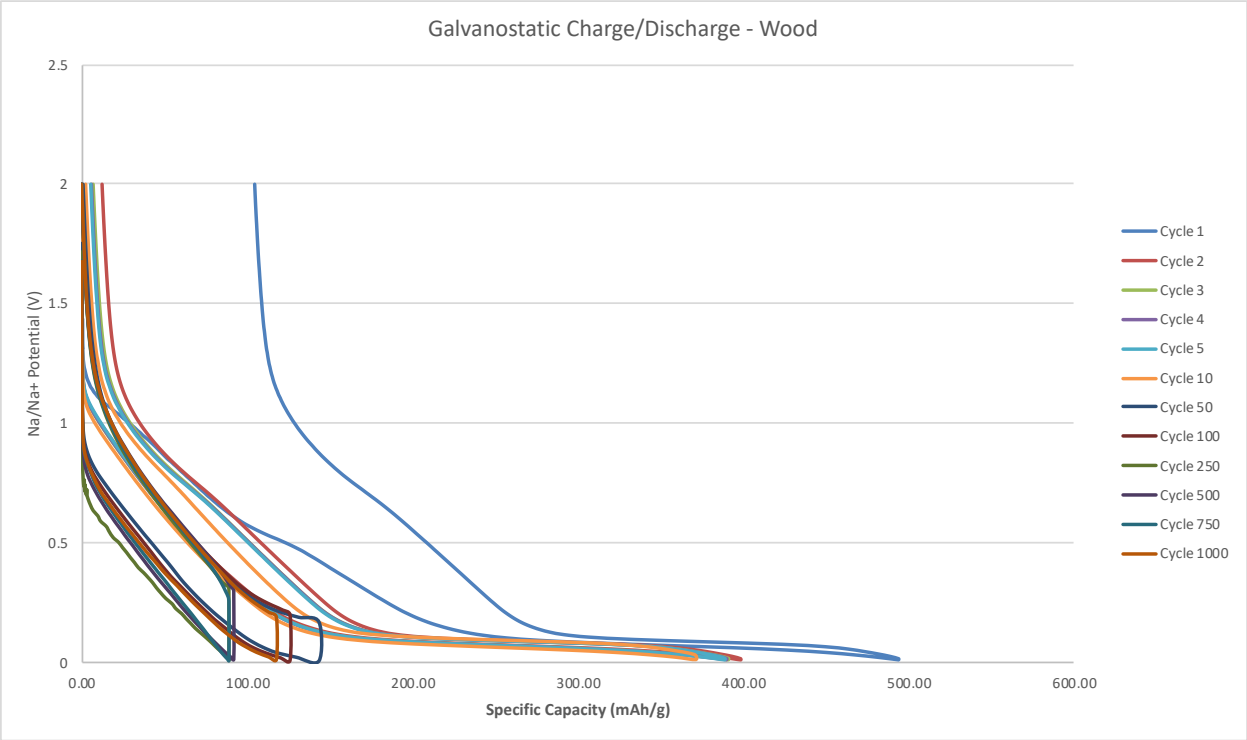

Figure 4.25 Galvanostatic charge/discharge cycles of selected cycles of wood.

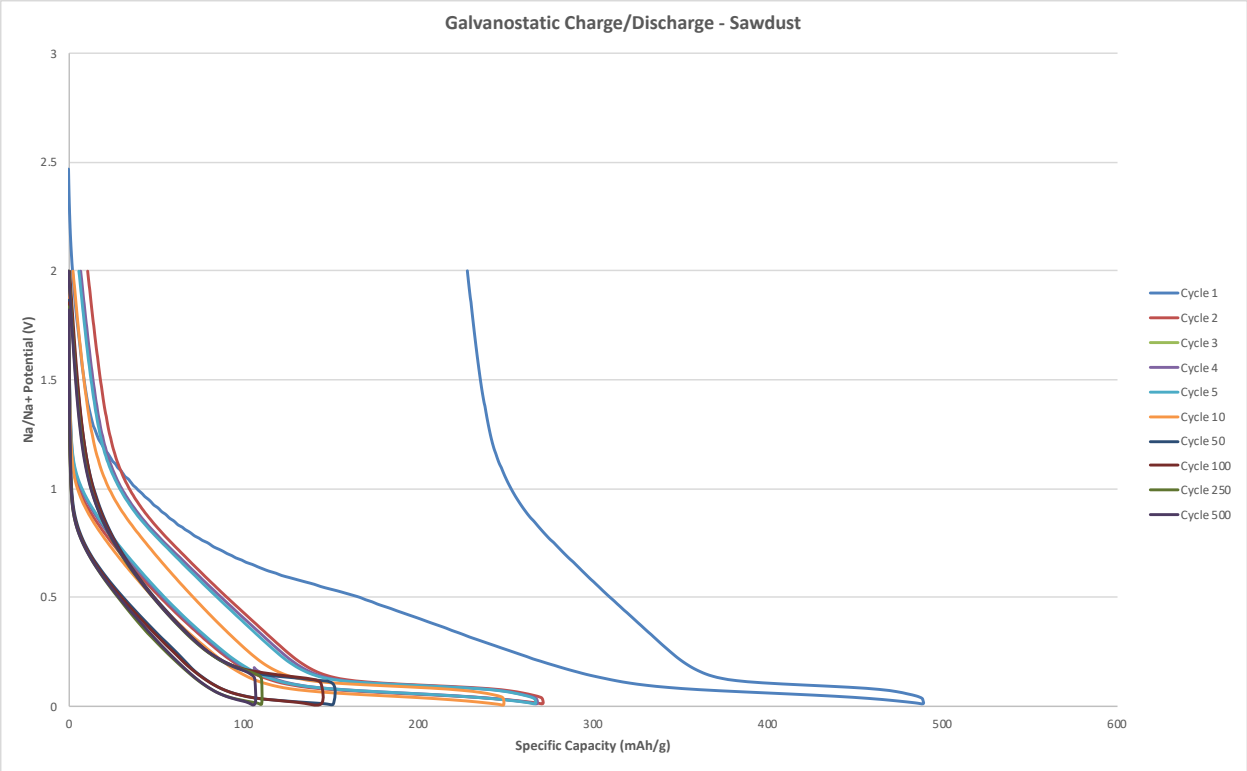

Figure 4.26 Galvanostatic charge/discharge cycles of selected cycles of sawdust.

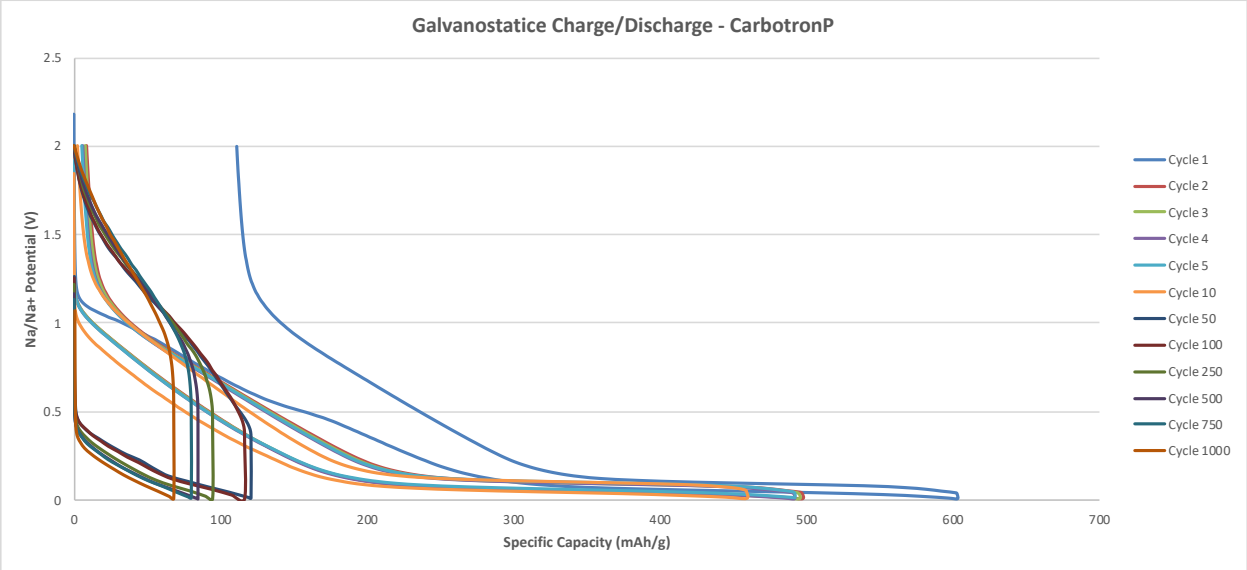

Figure 4.27 Galvanostatic charge/discharge cycles of selected cycles of CarbotronP.

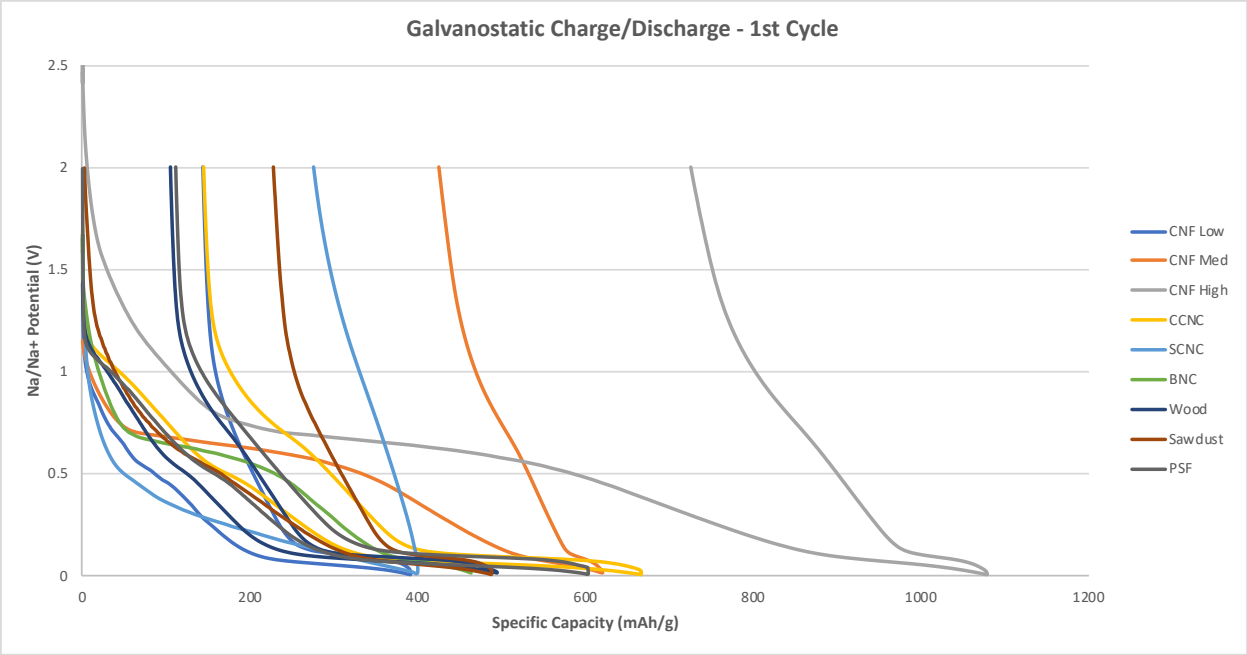

Figure 4.28 Galvanostatic charge/discharge curves of cycle 1 of all materials (Colors are same as 4.29).

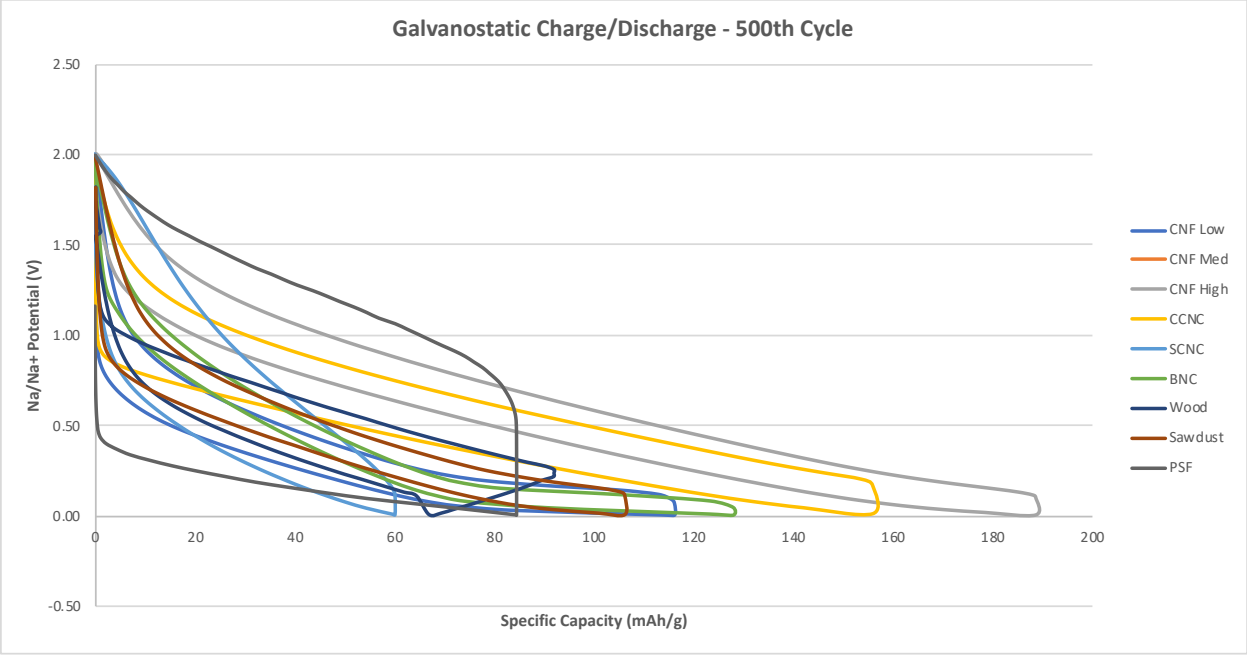

Figure 4.29 Galvanostatic charge/discharge curves of cycle 500 for all materials except CNF Med (Colors are same as 4.28).

Looking at Figure 4.28, CNF High shows the most pronounced SEI in comparison with its other cycles reaching 1078.9 mAh/g. CCNC Med Fib is the second closest with an SEI of nearly 700 mAh/g. The lowest SEI goes to CNF Low Fib at 390.94 mAh/g. The SEI is electrically insulating but allows for ionic movement. The SEI is thought to be an initial phase in which the ions tunnel in and form pathways for the future insertion cycles[25]. Lower SEI – such as the CNF low fib – indicate that the ions are either not tunneling or the sodium salts are too soluble to maintain a long insertion process, which is common in sodium ion batteries.

In Figure 4.29 CNF High Fib shows the largest specific capacity at 188.72 mAh/g. It has the highest SEI. CCNC has the second highest specific capacity and the highest SEI. This indicates that the insertion/desertion in cycling is highly related to the SEI forming pathways that allow for high electron movement. SCNC has the lowest specific capacity at the 500th cycle at 59.94 mAh/g. This shows that surface chemistry, not morphology has a potential effect of ionic movement within the battery.

4.4 – Long Term Cycling

Long term cycle testing was also conducted to test the batteries performance over 1000 cycles. Figure 4.30 shows a comparison of all of the long-term average cycling conducted for the batteries.

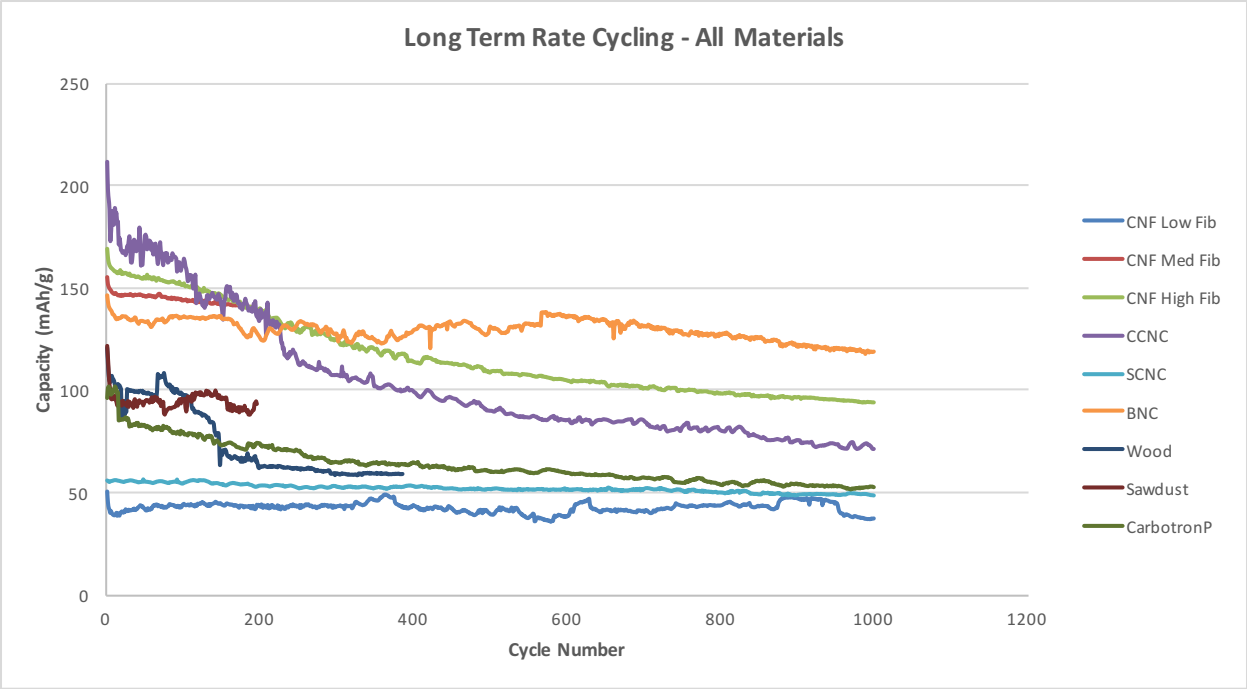

Figure 4.30 Long term cycling of all material types at 200 mAh/g over200-1000 cycles to test life of battery by comparing cycles to capacity.

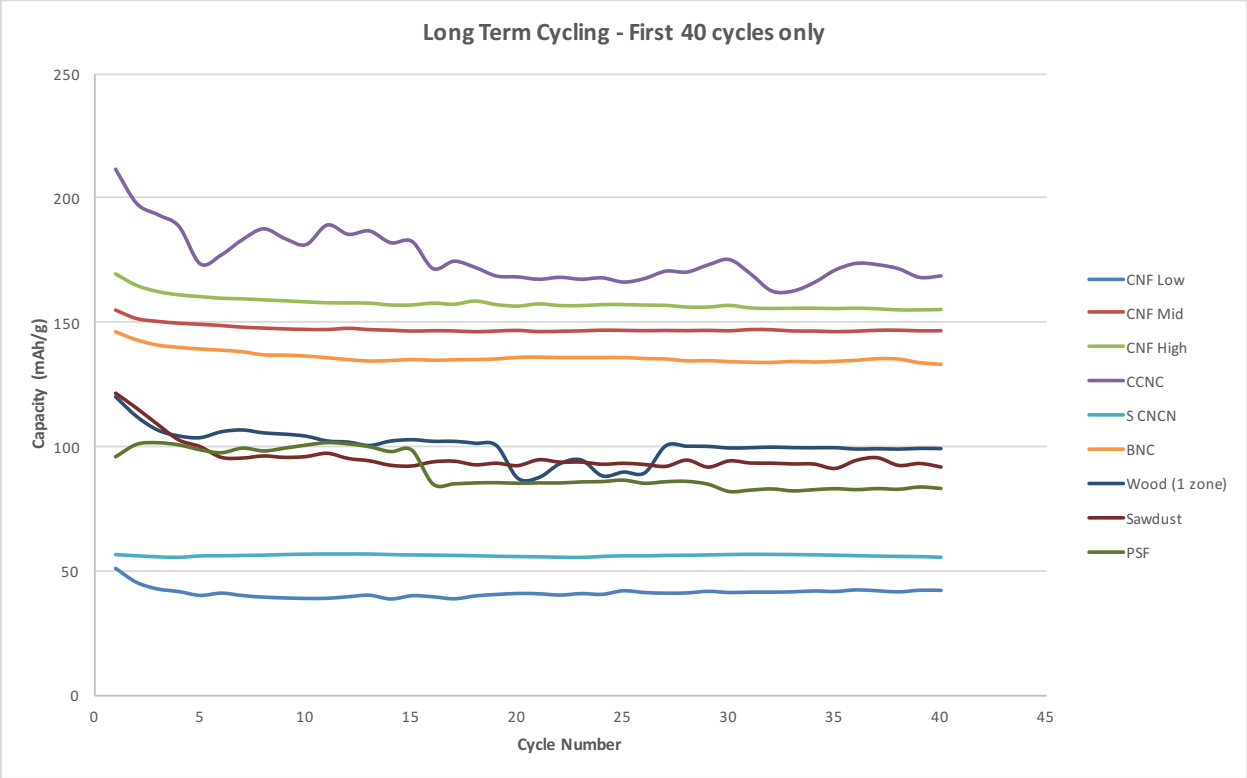

Figure 4.31 First 40 cycles of long term cycling for all materials at 200 mAh/g.

BNC performs the best maintaining a high capacity over the course of 1000 cycles. CNF Low Fib performs more like a capacitor than a battery, showing a steady, but low cycling profile. CCNC performs well for the first few cycles but the rapid loss of capacity makes it a poor choice for a lifelong anode. SCNC, unlike CCNC, has a constant performance, but like CNF Low Fib, it has a low capacity and thus performs more like a capacitor than a battery. CarbotronP, the industry standard currently, performs similarly to CCNC, but at a lower capacity than CCNC. The macro controls of wood and sawdust performed in the same capacity window as CarbotronP. Wood has a profile similar to that of CCNC but more extreme and condensed.

Comparing the above two figures (4.30, and 4.31) with Figure 4.28, there does not appear to be any strong correlations between a low or high SEI and long-term cycling with the exception of the first 40 cycles of CCNC. CCNC performs well for the first 40 cycles, but then declines rapidly. BNC, and CNF Low Fib – both of which have low SEIs – performed consistently but differently. Again, CNF Low Fib performing more like a capacitor, and BNC having a sustained and ultimately best long-term cycling performance.

Chapter 5 – Conclusion

Energy storage is much needed as renewable energy sources grow. Lithium Ion batteries are the current gold standard of our battery technology, but they are too expensive to be used for mass storage, and the supply is decreasing. An abundance of sodium allows for large battery construction, and the properties of nanocellulose allow for mass storage batteries to be a reality.

Long term cycling showed that bacterial nanocellulose is an ideal anode with steady cycling over 1000 cycles at a high capacity. If a low capacity is desired and/or can be tolerated, Low Fib CNF is shown to be ideal for an anode material as it is shown to be nearly constant over 2000 cycles. Low Fib CNF is also easier and less expensive to produce than BNC. This could make it a strong contender. There is more work to be done with the solid electrolyte interphase, but with research in this field rapidly expanding, the problems of solubility within the batteries appears to be solvable.

Overall, using nanocellulose as a starting material for a hard carbon anode in sodium ion batteries allows for long lasting anodes and performance in SIBs that have not been seen prior.

Bibliography

[1] A. Volta, "On the Electricity Excited by the Mere Contact of Conducting Substances of Different Kinds . In a Letter from Mr . Alexander Volta , F . R . S . Professor of Natural Philosophy in the University of Pavia , to the Rt . Hon . Sir Joseph Banks , Bart . K . B," *Philos. Trans. R. Society London*, vol. 90, no. 1800, pp. 403–431, 1990.

[2] C. Daniel and J. O. Besenhard, *Handbook of Battery Materials: Second Edition*. 2011.

[3] L. Lu, X. Han, J. Li, J. Hua, and M. Ouyang, "A review on the key issues for lithium-ion battery management in electric vehicles," *J. Power Sources*, vol. 226, pp. 272–288, Mar. 2013.

[4] R. J. Moon, A. Martini, J. Nairn, J. Simonsen, and J. Youngblood, "Cellulose nanomaterials review: structure, properties and nanocomposites.," *Chem. Soc. Rev.*, vol. 40, no. 7, pp. 3941–94, Jul. 2011.

[5] P. W. Atkins, "Shriver & Atkins' inorganic chemistry," *Shriver Atkin's Inorg. Chem.*, p. 851, 2010.

[6] Z. Q. Li, C. J. Lu, Z. P. Xia, Y. Zhou, and Z. Luo, "X-ray diffraction patterns of graphite and turbostratic carbon," *Carbon N. Y.*, vol. 45, no. 8, pp. 1686–1695, Jul. 2007.

[7] K. Dasgupta and D. Sathiyamoorthy, "Disordered carbon–its preparation, structure, and characterisation," *Mater. Sci. Technol.*, vol. 19, no. 8, pp. 995–1002, Aug. 2003.

[8] D. A. Stevens and J. R. Dahn, "High Capacity Anode Materials for Rechargeable Sodium-Ion Batteries," *J. Electrochem. Soc.*, vol. 147, no. 4, p. 1271, Apr. 2000.

[9] D. Kundu, E. Talaie, V. Duffort, and L. F. Nazar, "The Emerging Chemistry of Sodium Ion Batteries for Electrochemical Energy Storage," *Angew. Chemie Int. Ed.*, vol. 54, no. 11, p. n/a-n/a, Feb. 2015.

[10] S. Brunauer, P. H. Emmett, and E. Teller, "Adsorption of Gases in Multimolecular Layers," *J. Am. Chem. Soc.*, vol. 60, no. 2, pp. 309–319, 1938.

[11] M. D. Slater, D. Kim, E. Lee, and C. S. Johnson, "Sodium-ion batteries," *Adv. Funct. Mater.*, vol. 23, no. 8, pp. 947–958, 2013.

[12] N. Yabuuchi, K. Kubota, M. Dahbi, and S. Komaba, "Research development on sodium-ion batteries.," *Chem. Rev.*, vol. 114, no. 23, pp. 11636–11682, 2014.

[13] W. Luo, J. Schardt, C. Bommier, B. Wang, J. Razink, J. Simonsen, and X. Ji, "Carbon nanofibers derived from cellulose nanofibers as a long-life anode material for rechargeable sodium-ion batteries," *J. Mater. Chem. A*, vol. 1, no. 36, pp. 10662–10666, 2013.

[14] S. Komaba, W. Murata, T. Ishikawa, N. Yabuuchi, T. Ozeki, T. Nakayama, A. Ogata, K. Gotoh, and K. Fujiwara, "Electrochemical Na insertion and solid electrolyte interphase for hard-carbon electrodes and application to Na-ion batteries," *Adv. Funct. Mater.*, vol. 21, no. 20, pp. 3859–3867, 2011.

[15] A. Ponrouch, E. Marchante, M. Courty, J.-M. Tarascon, and M. R. Palacín, "In search of an optimized electrolyte for Na-ion batteries," *Energy Environ. Sci.*, vol. 5, no. 9, p. 8572, Aug. 2012.

[16] H. Pan, Y.-S. Hu, and L. Chen, "Room-temperature stationary sodium-ion batteries for large-scale electric energy storage," *Energy Environ. Sci.*, vol. 6, no. 8, p. 2338, Jul. 2013.

[17] J. K. Pandey, A. N. Nakagaito, and H. Takagi, "Fabrication and applications of cellulose nanoparticle-based polymer composites," *Polymer Engineering and Science*, vol. 53, no. 1. pp. 1–8, 2013.

[18] J. H. Kim, B. S. Shim, H. S. Kim, Y. J. Lee, S. K. Min, D. Jang, Z. Abas, and J. Kim, "Review

of nanocellulose for sustainable future materials," *International Journal of Precision Engineering and Manufacturing - Green Technology*, vol. 2, no. 2. pp. 197–213, 2015.

[19] L. Wang, C. Schütz, G. Salazar-Alvarez, and M.-M. Titirici, "Carbon aerogels from bacterial nanocellulose as anodes for lithium ion batteries," *RSC Adv.*, vol. 4, no. 34, p. 17549, Apr. 2014.

[20] M. Pääkkö, J. Vapaavuori, R. Silvennoinen, H. Kosonen, M. Ankerfors, T. Lindström, L. A. Berglund, and O. Ikkala, "Long and entangled native cellulose I nanofibers allow flexible aerogels and hierarchically porous templates for functionalities," *Soft Matter*, vol. 4, no. 12, p. 2492, Nov. 2008.

[21] M. A. Meyers, A. Mishra, and D. J. Benson, "Mechanical properties of nanocrystalline materials," *Progress in Materials Science*, vol. 51, no. 4. pp. 427–556, 2006.

[22] Y. Zhai, Y. Dou, D. Zhao, P. F. Fulvio, and R. T. Mayes, "Carbon Materials for Chemical Capacitive Energy Storage," *Adv. Mater.*, vol. 23, no. 42, pp. 4828–4850, 2011.

[23] M. S. Islam and C. A. J. Fisher, "Lithium and sodium battery cathode materials: computational insights into voltage, diffusion and nanostructural properties.," *Chem. Soc. Rev.*, vol. 43, no. 1, pp. 185–204, 2014.

[24] M. . Tang and R. Bacon, "Carbonization of cellulose fibers—I. Low temperature pyrolysis," *Carbon N. Y.*, vol. 2, no. 3, pp. 211–220, 1964.

[25] R. Morgensen, D. Brandell, and R. Younesi, "Solubility of the SOlid Electrolyte Interphase (SEI) in Sodium Ion Batteries," *ACS Energy Lett.*, vol. 1, no. 6, pp. 1173–1178, 2016.

Appendix A - Conductivity titration and data for CCNC Sample

Figure A1 below shows a standard conductivity plot obtained for CCNC carboxyl group titrations. There are three colors indicating the three slopes of the acid/base titration. The red points indicate the HCl neutralizing, the green is the base (NaOH) equilibrating, and the purple points show the excess base. The intersections of these curves are extrapolated by the linear trendlines to determine accurate values for the mmol carboxyl group per grams of cellulose.

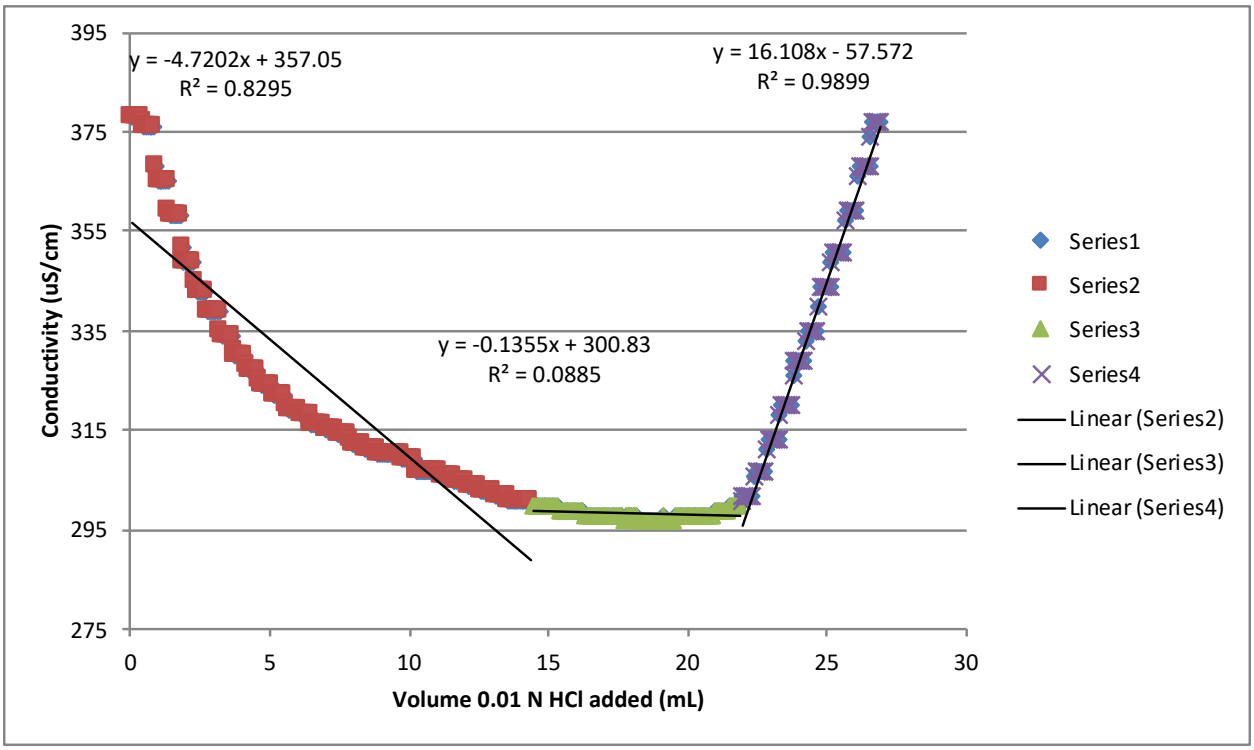

Figure A.1 Sample conductivity titration plot of CCNC.

In the example above, the mass of the CCNC solution was 17.0621 g, the percent solids of CCNC was 0.0165%, thus making the CCNC mass 0.2815 g. Using the data from the linear trendlines found in Figure A.1, the following formula was applied

$$\left[\frac{(int.\,base - int.\,titration)}{(slope\ titration - slope\ base)} - \frac{(int.\,base - int\ base\ titration)}{(slope\ b.titration - slope\ base)}\right] \times \left(\frac{0.0101}{CCNC\ mass}\right)$$

The numerical calculation gave a value of 0.3517 mmol carboxyl / g cellulose.